Essential Dynamics of the Vertical Wind Shear Affecting the Secondary Eyewall Formation in Tropical Cyclones

Yi-Fan Wang and Zhe-Min Tan

JAS (2022)

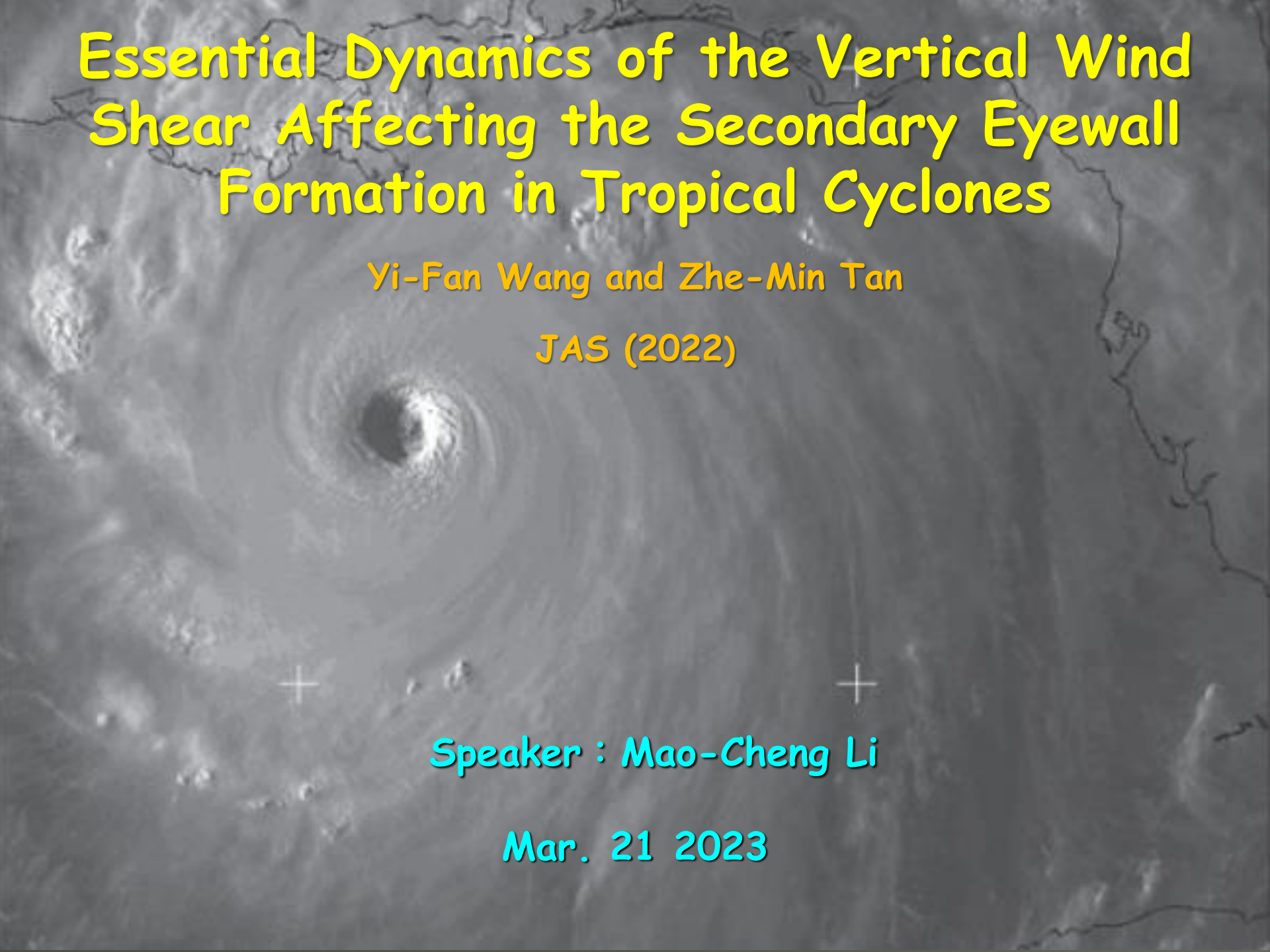

Speaker : Mao-Cheng Li

Mar. 21 2023

Outline

- Introduction
- Model setup and experiment design
- Overview and results
- Evolution and BL response of rainbands at left of shear
- Convection initiation at UR
- Discussion and Conclusions

1. Introduction

- The impacts of VWS on SEF are still unclear. Despite the SEF climatology indicating that SEF corresponds with weaker VWS (Kossin and Sitkowski 2009), cases of SEF under strong VWS are also documented in observational studies (Zhang and Perrie 2018; Dougherty et al. 2018). In idealized simulation studies, Zhang et al. (2017) found that 38 out of 40 members undergo complete or partial SEF under VWS of 6 m s^−1, indicating that sheared environmental conditions do not prevent SEF. As a result, the influence of VWS on SEF is still debatable.

- Recent studies have widely acknowledged the initiating role of the asymmetric forcing associated outer rainbands (ORBs) in SEF (Qiu and Tan 2013; Didlake et al. 2018; Wang et al. 2019; WT20). Compared to inner rainbands, ORBs exhibit asymmetric structures that consist of convective precipitation at the upwind and stratiform precipitation at the downwind end (Moon and Nolan 2010; Didlake and Houze 2013b).

- Qiu and Tan (2013) first identified that the asymmetric inflow at the downwind portion of ORBs descends into boundary layer (BL) and helps initiate convection during the early stage of SEF. The existence and role of the descending inflow in triggering convection were corroborated by observations of Hurricane Earl (2010) (Didlake et al. 2018). Wang et al. (2019) emphasized that the axisymmetrization of asymmetric winds associated with ORBs contributes to accelerating the secondary tangential wind maximum of SEF.

1. Introduction cont.

- WT20 pointed out that the asymmetric radial inflow reinforces BL convergence and stretches up the BL relative vorticity at the radially inward side of ORBs, which was a crucial point in the development of the secondary convective ring and the BL tangential wind maximum. In comparison, the vortex dominated by inner rainbands fails to drive the secondary tangential wind maximum pathways, demonstrating the ORBs are the internal triggering mechanism of SEF.

- A canonical SEF, based on previous observations and simulations, should have two basic characteristics: a secondary convective ring and an associated secondary low-level tangential wind maximum. The influence on both two features should be taken into consideration when assessing the impact of VWS on SEF. Moreover, because the asymmetric forcing of ORBs is vital to SEF, the effect of VWS on ORBs can be viewed as a starting point for investigating the influences on SEF.

- Typically, the convective cells of ORBs develop at DR quadrant, mature at downshear-left (DL) quadrant, and collapse into stratiform at upshear-left (UL) quadrant, which respectively corresponds to the upwind, middle, and downwind portions of the ORBs (Hence and Houze 2008). In this regard, VWS facilitates the development of ORBs and fixes the structures of ORBs in shear-relative quadrants, providing the asymmetric forcing necessary for SEF.

- While the VWS may facilitate the asymmetric forcing of ORBs for SEF at the downshear side, the projection of asymmetric forcing onto the axisymmetric state is more difficult under VWS. Therefore, the effects of VWS on SEF should be bifurcated and dependent on the magnitudes of VWS.

1. Introduction cont.

- Based on the above questions, the impacts of VWS on SEF and associated dynamics are being investigated in this study, aiming to answer the following questions:

1. How does VWS with varying magnitudes affect SEF?
2. How do the structures of ORBs and BL responses related to SEF evolve in different VWS-relative quadrants?
3. How do the secondary convective ring and tangential wind maximum form at upshear side under VWS?

2. Model setup and experiment design

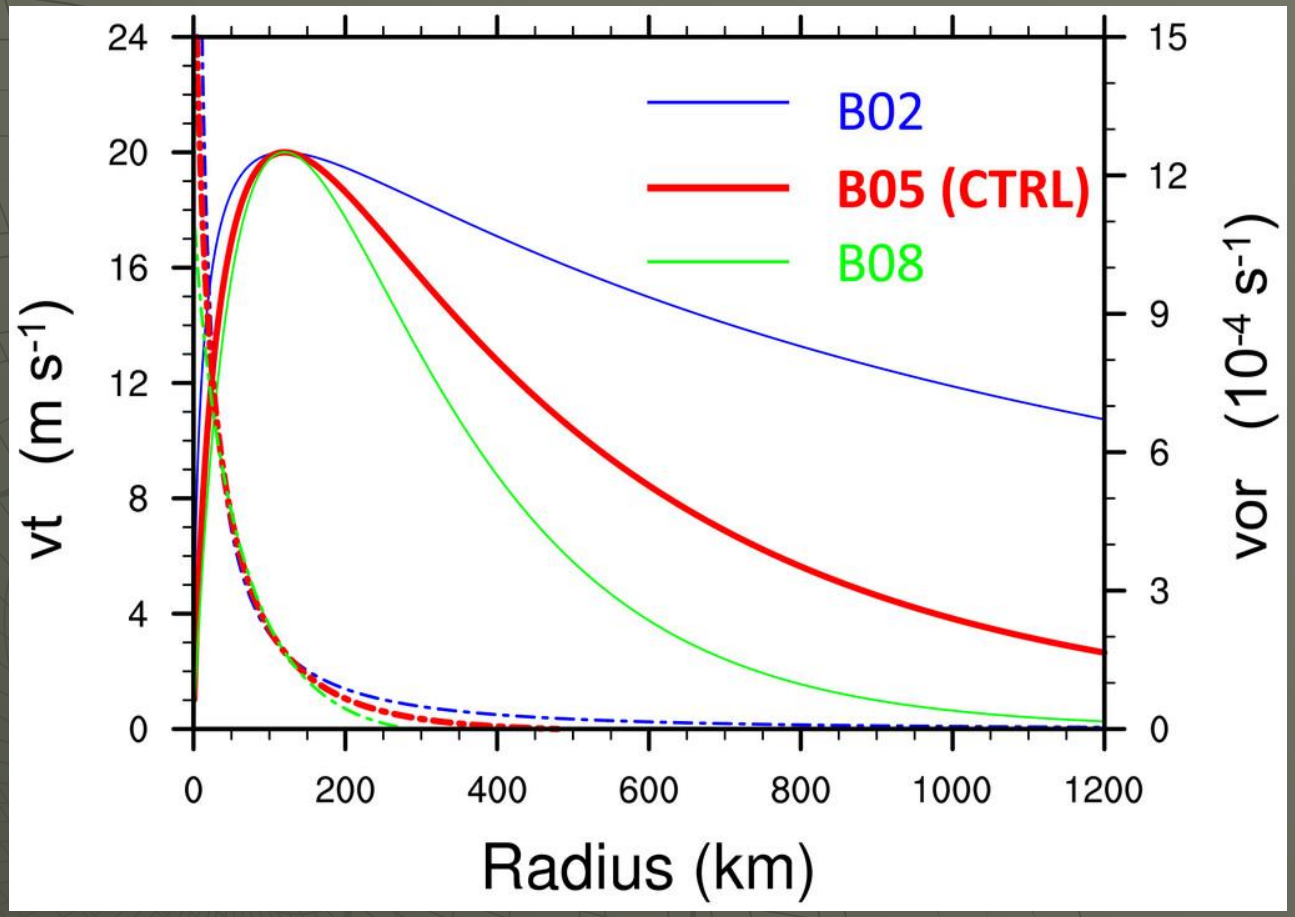

- In this study, B05 is chosen as the control run (CTRL) to assess the influence of VWS on SEF. VWSs of varying magnitudes are added on B05 to determine whether VWSs are beneficial to SEF by inducing the formation of the secondary tangential wind maximum, or detrimental to SEF by breaking the secondary convective ring.

2. Model setup and experiment design cont.

- The initial vortex is integrated with Weather Research and Forecasting (WRF) Model (version 3.8.1) on an f plane at 20°N over a quiescent ocean with a constant SST of 28°C.
- There are three nested domains (361 × 361, 181 × 181, 361 × 361) with horizontal grid spacing of 18, 6, and 2 km, respectively.
- The parameterization schemes are identical to those used in WT20, including the Thompson (Thompson et al. 2004, 2008) and the Mellor–Yamada–Janjić (MYJ) (Janjić 1996, 2002) for the parameterization of the microphysical and planetary boundary layer processes, respectively.
- The RRTM longwave (Mlawer et al. 1997); and Goddard shortwave radiative scheme (Chou and Suarez 1999).
- The Kain–Fritch cumulus scheme (Kain 2004) is applied in the outer two domains.

2. Model setup and experiment design cont.

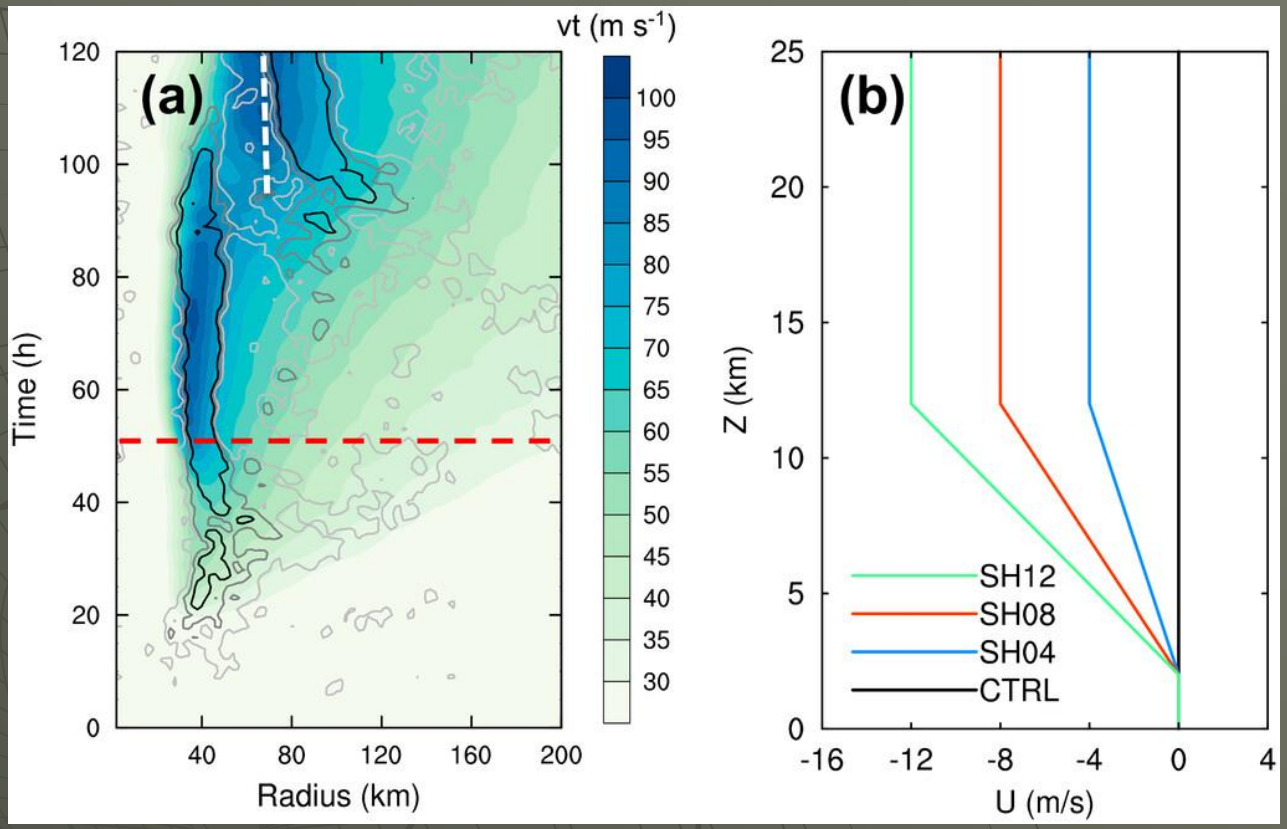

- VWS is introduced at 48 h when the simulated storm is formed in CTRL.
- Shear magnitudes of 4, 8, and 12 m s^−1 are adopted to represent the weak, moderate, and strong VWS, respectively (Rios-Berrios and Torn 2017).
- Adopt the vertical profiles of the zonal wind, which changes linearly between the heights of 2 and 12 km with zero flow in the lower levels, since we mainly focus on the influence of shear magnitudes in this study.

3. Overview and results —— a. Axisymmetric evolution

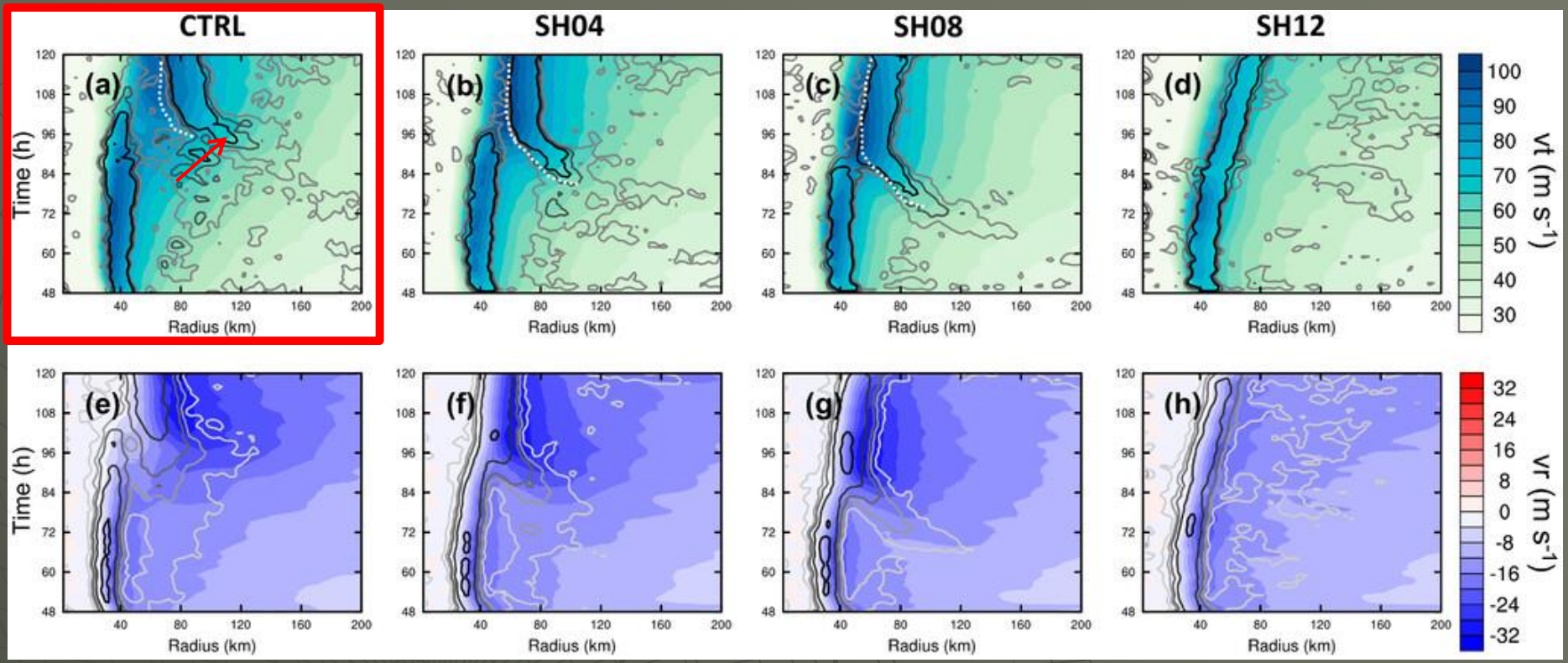

- (a)–(d) Time–radius evolution of the azimuthal-mean tangential wind at z = 1 km (m s^−1, shading) overlaid with the vertical velocity z = 5 km (m s^−1, contours at 0.25, 0.5 and 1.0 m s^−1) during 48–120 h.

- (e)–(h) As in (a)–(d), but showing the BL inflow (m s^−1, averaged between z = 0.2–1 km, shading) overlaid with the divergence (contours at −1, −3, −5, −10, and −20 × 10^−4 s^−1, averaged between z = 0.2 and 1 km). The secondary RMW is marked by white dashed lines.

3. Overview and results —— a. Axisymmetric evolution cont.

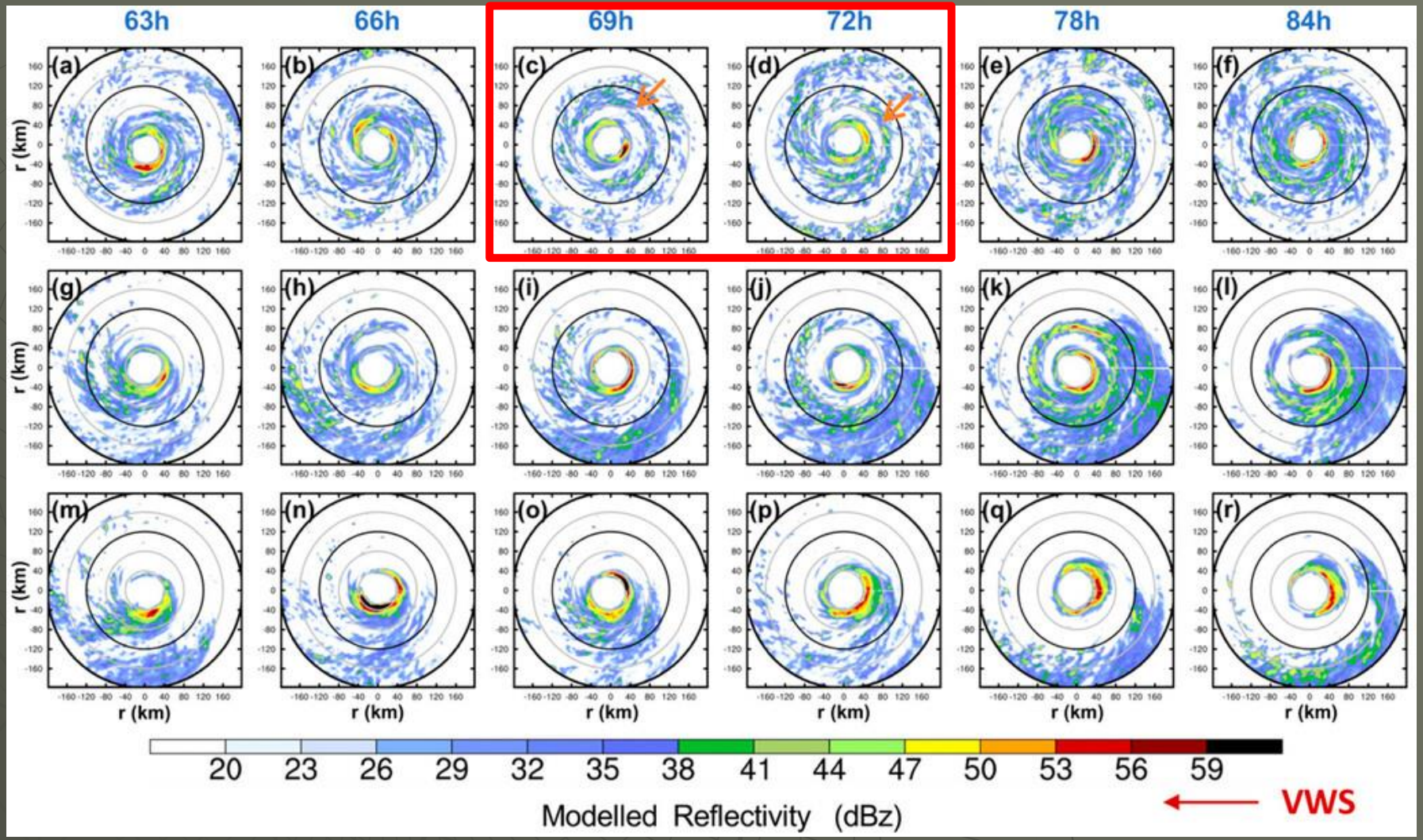

- Plan view of the modeled reflectivity (dBZ) at z = 3 km during 63–84 h. (a)–(f) CTRL, (g)–(l) SH08, and (m)–(r) SH12. Circles are shown at every 40 km from the storm center and the black circle highlights the 120 km radius. The red arrow indicates the shear direction. The orange arrows indicate the secondary convective ring in CTRL.

3. Overview and results —— a. Axisymmetric evolution cont.

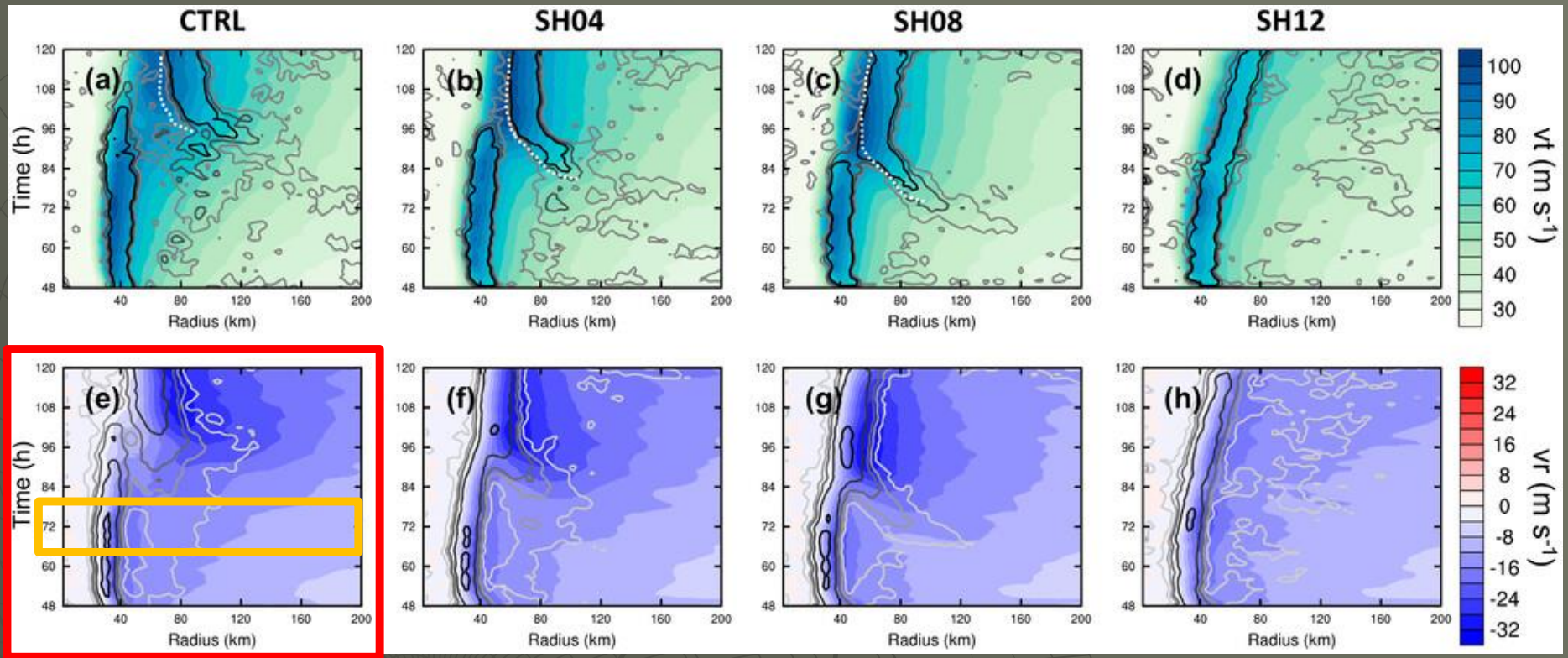

- (a)–(d) Time–radius evolution of the azimuthal-mean tangential wind at z = 1 km (m s^−1, shading) overlaid with the vertical velocity z = 5 km (m s^−1, contours at 0.25, 0.5 and 1.0 m s^−1) during 48–120 h.

- (e)–(h) As in (a)–(d), but showing the BL inflow (m s^−1, averaged between z = 0.2–1 km, shading) overlaid with the divergence (contours at −1, −3, −5, −10, and −20 × 10^−4 s^−1, averaged between z = 0.2 and 1 km). The secondary RMW is marked by white dashed lines.

3. Overview and results —— a. Axisymmetric evolution cont.

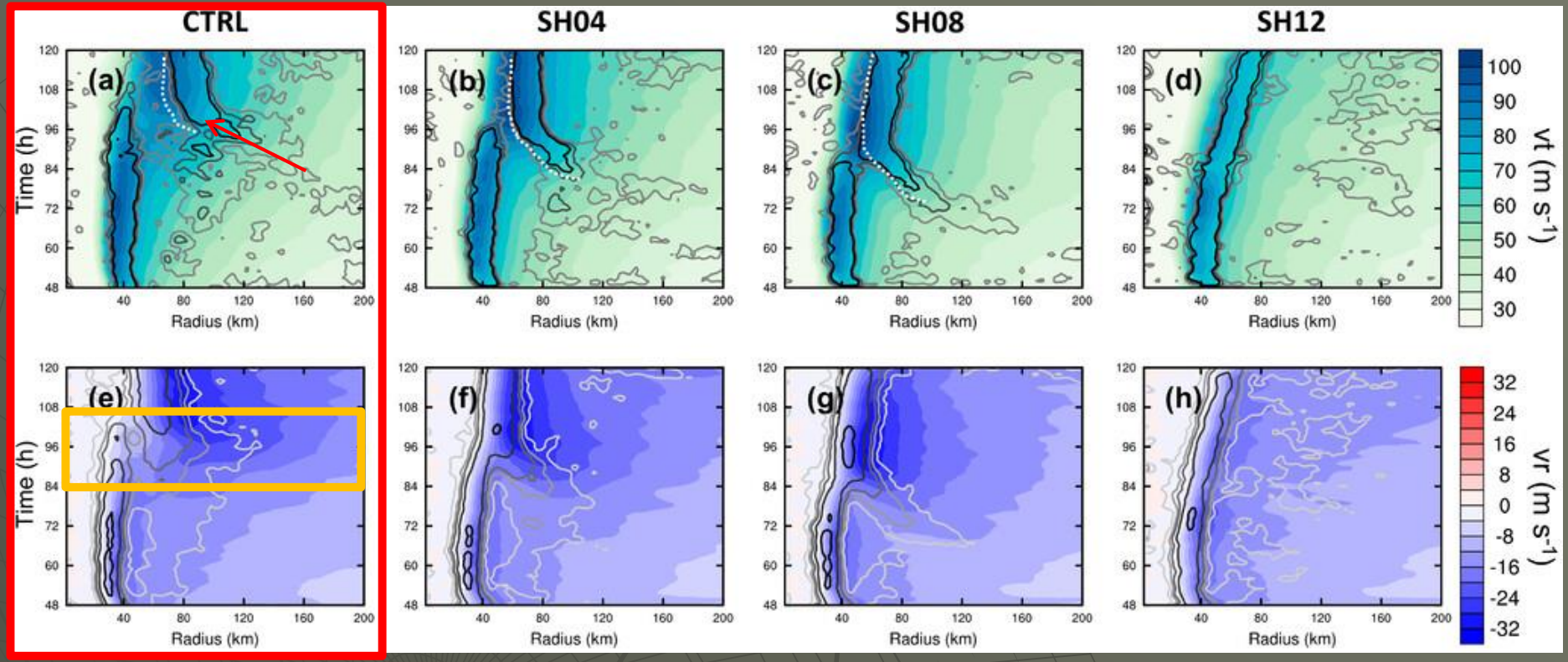

- (a)–(d) Time–radius evolution of the azimuthal-mean tangential wind at z = 1 km (m s^−1, shading) overlaid with the vertical velocity z = 5 km (m s^−1, contours at 0.25, 0.5 and 1.0 m s^−1) during 48–120 h.

- (e)–(h) As in (a)–(d), but showing the BL inflow (m s^−1, averaged between z = 0.2–1 km, shading) overlaid with the divergence (contours at −1, −3, −5, −10, and −20 × 10^−4 s^−1, averaged between z = 0.2 and 1 km). The secondary RMW is marked by white dashed lines.

3. Overview and results —— a. Axisymmetric evolution cont.

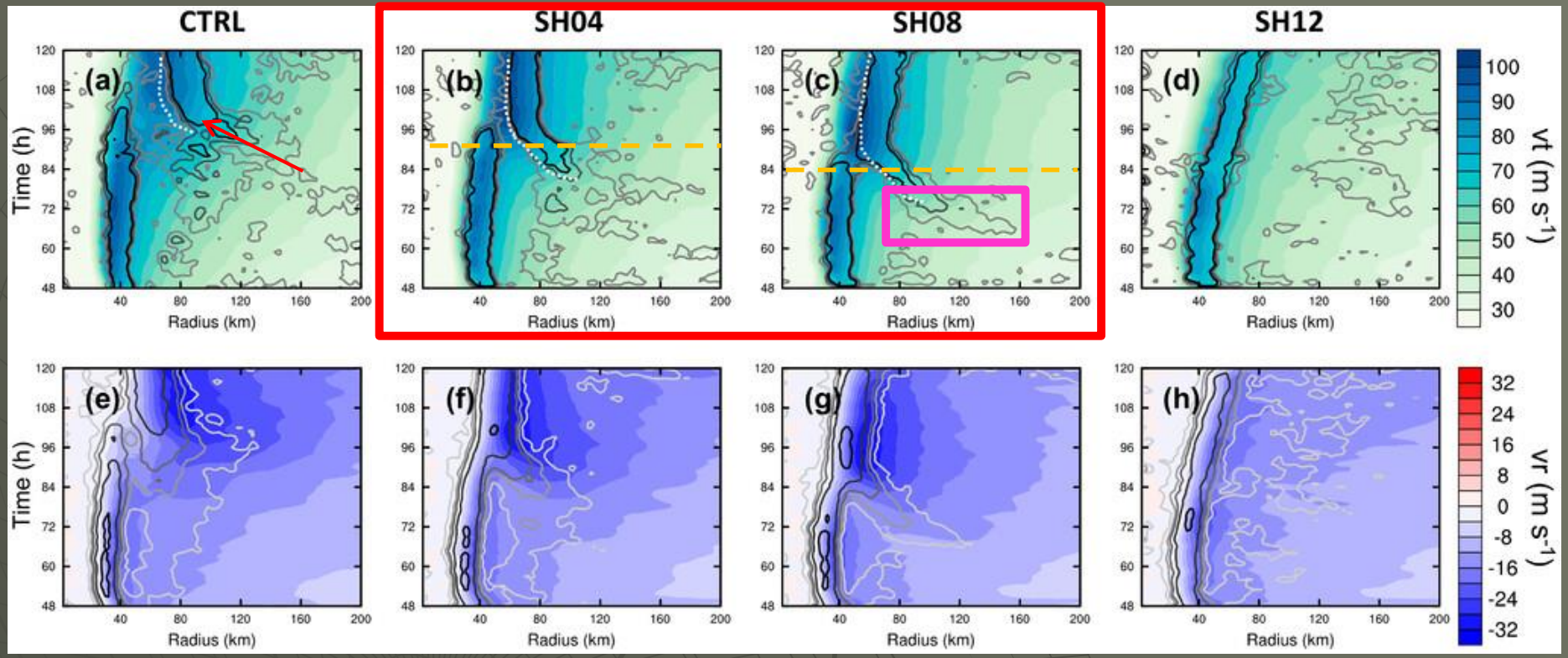

- (a)–(d) Time–radius evolution of the azimuthal-mean tangential wind at z = 1 km (m s^−1, shading) overlaid with the vertical velocity z = 5 km (m s^−1, contours at 0.25, 0.5 and 1.0 m s^−1) during 48–120 h.

- (e)–(h) As in (a)–(d), but showing the BL inflow (m s^−1, averaged between z = 0.2–1 km, shading) overlaid with the divergence (contours at −1, −3, −5, −10, and −20 × 10^−4 s^−1, averaged between z = 0.2 and 1 km). The secondary RMW is marked by white dashed lines.

3. Overview and results —— a. Axisymmetric evolution cont.

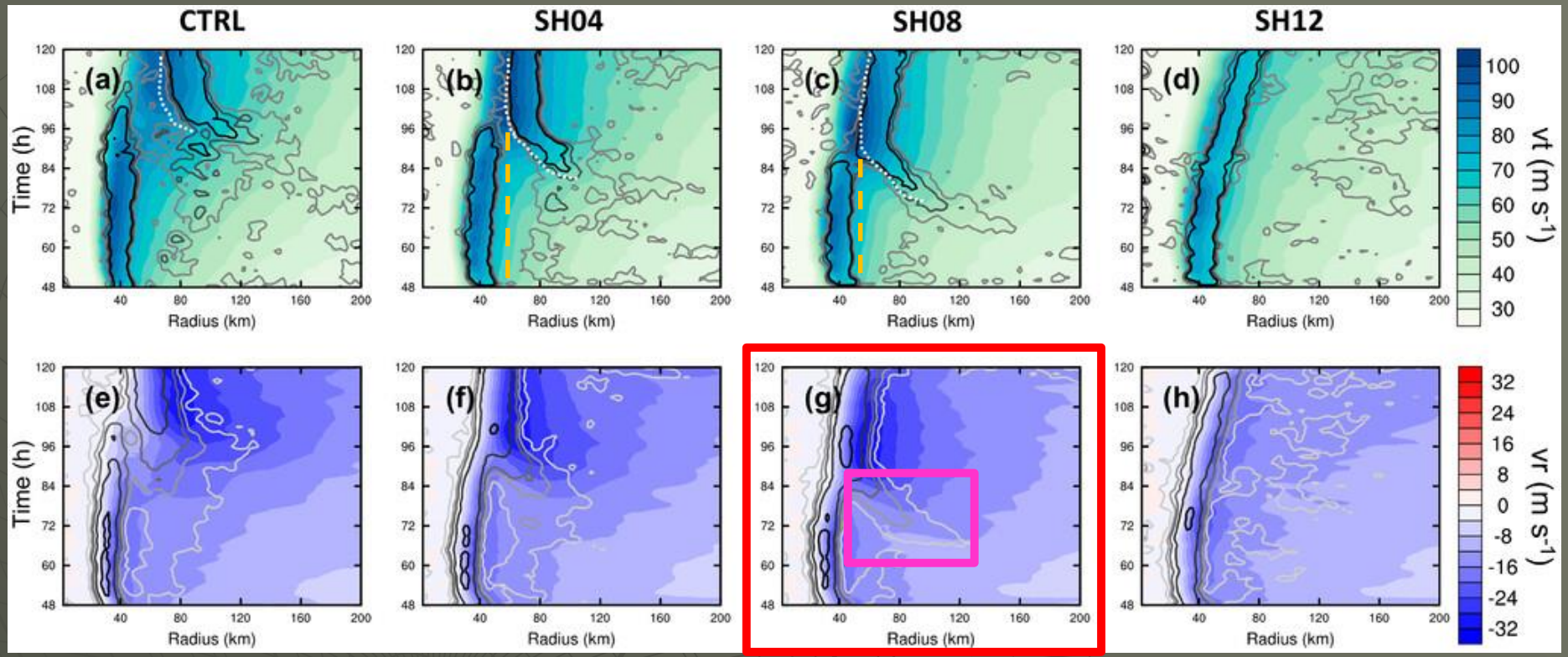

- (a)–(d) Time–radius evolution of the azimuthal-mean tangential wind at z = 1 km (m s^−1, shading) overlaid with the vertical velocity z = 5 km (m s^−1, contours at 0.25, 0.5 and 1.0 m s^−1) during 48–120 h.

- (e)–(h) As in (a)–(d), but showing the BL inflow (m s^−1, averaged between z = 0.2–1 km, shading) overlaid with the divergence (contours at −1, −3, −5, −10, and −20 × 10^−4 s^−1, averaged between z = 0.2 and 1 km). The secondary RMW is marked by white dashed lines.

3. Overview and results —— a. Axisymmetric evolution cont.

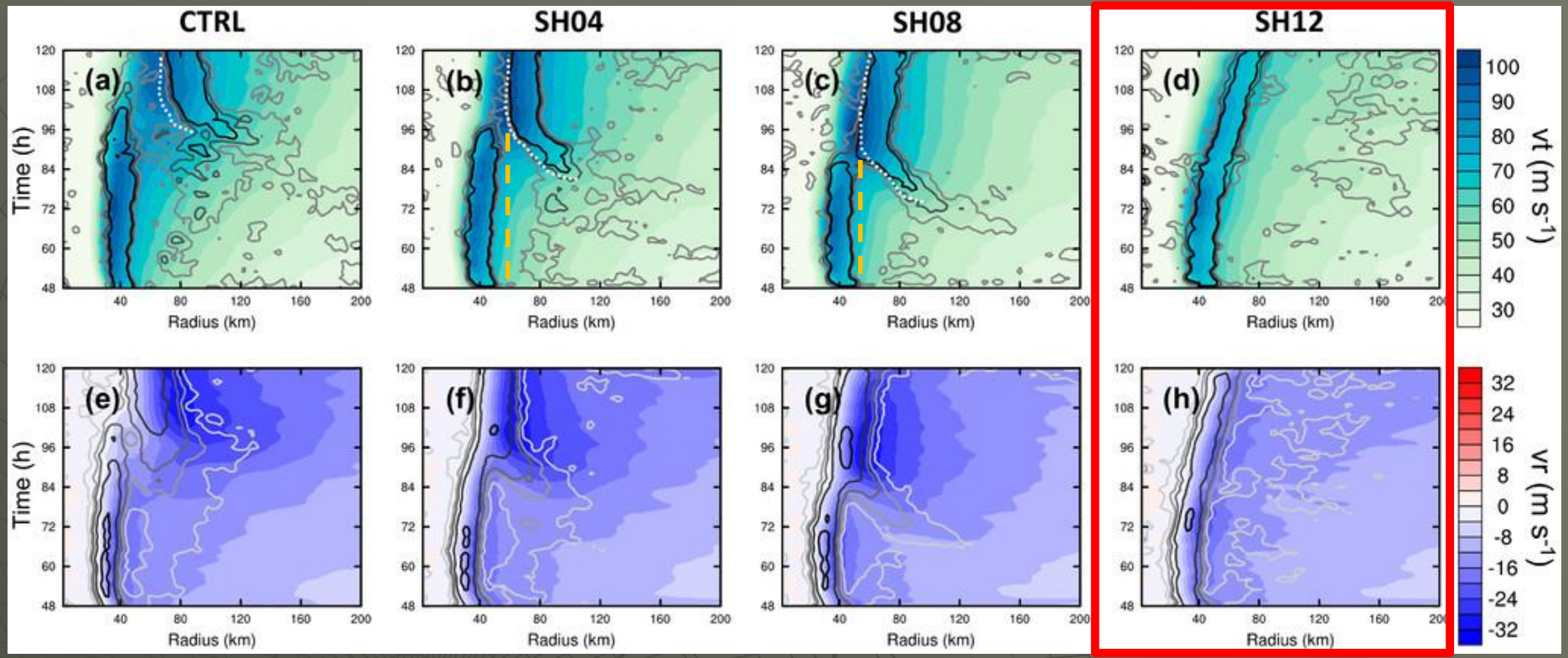

- (a)–(d) Time–radius evolution of the azimuthal-mean tangential wind at z = 1 km (m s^−1, shading) overlaid with the vertical velocity z = 5 km (m s^−1, contours at 0.25, 0.5 and 1.0 m s^−1) during 48–120 h.

- (e)–(h) As in (a)–(d), but showing the BL inflow (m s^−1, averaged between z = 0.2–1 km, shading) overlaid with the divergence (contours at −1, −3, −5, −10, and −20 × 10^−4 s^−1, averaged between z = 0.2 and 1 km). The secondary RMW is marked by white dashed lines.

3. Overview and results —— b. Rainbands evolution

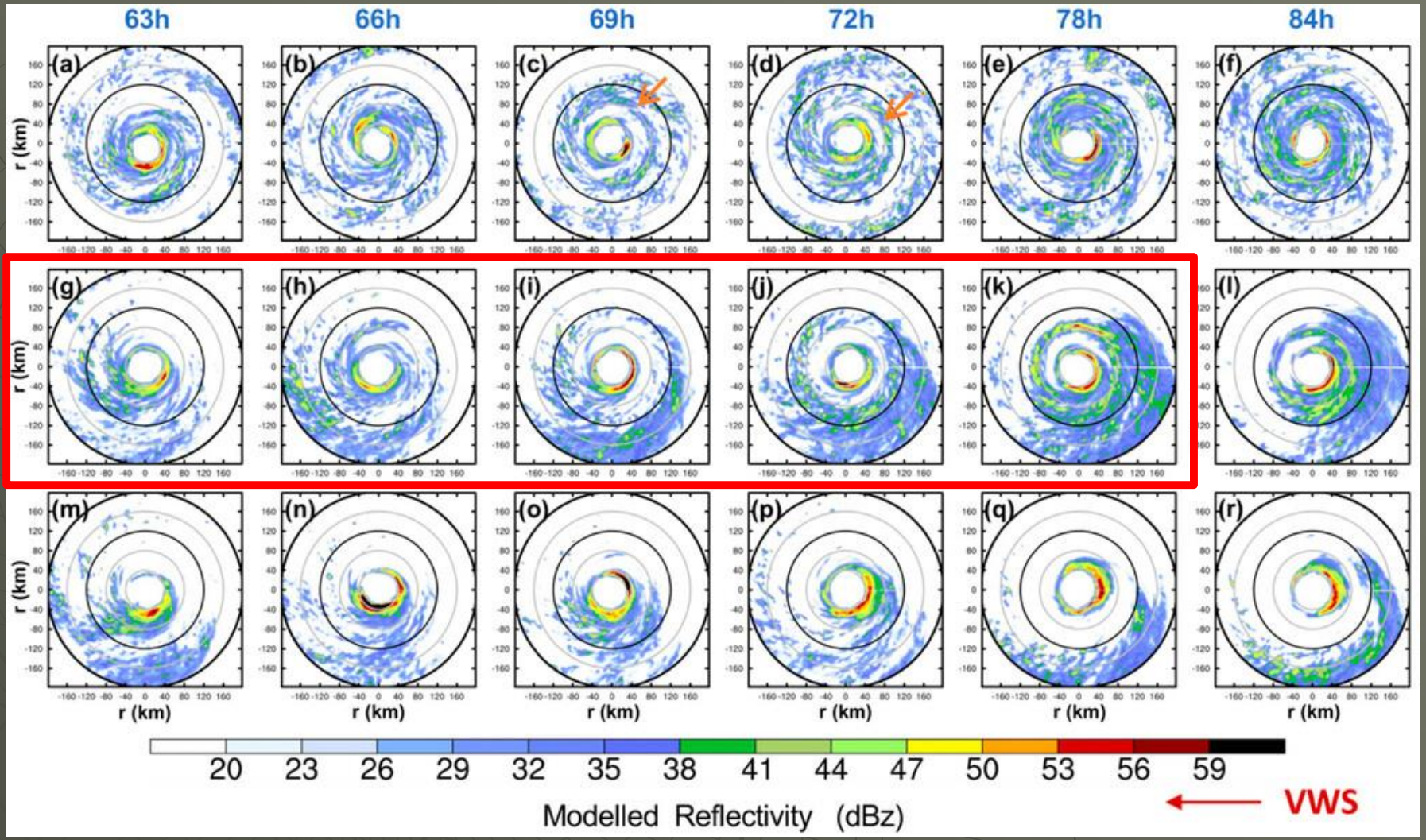

- Plan view of the modeled reflectivity (dBZ) at z = 3 km during 63–84 h. (a)–(f) CTRL, (g)–(l) SH08, and (m)–(r) SH12. Circles are shown at every 40 km from the storm center and the black circle highlights the 120 km radius. The red arrow indicates the shear direction. The orange arrows indicate the secondary convective ring in CTRL.

3. Overview and results —— b. Rainbands evolution cont.

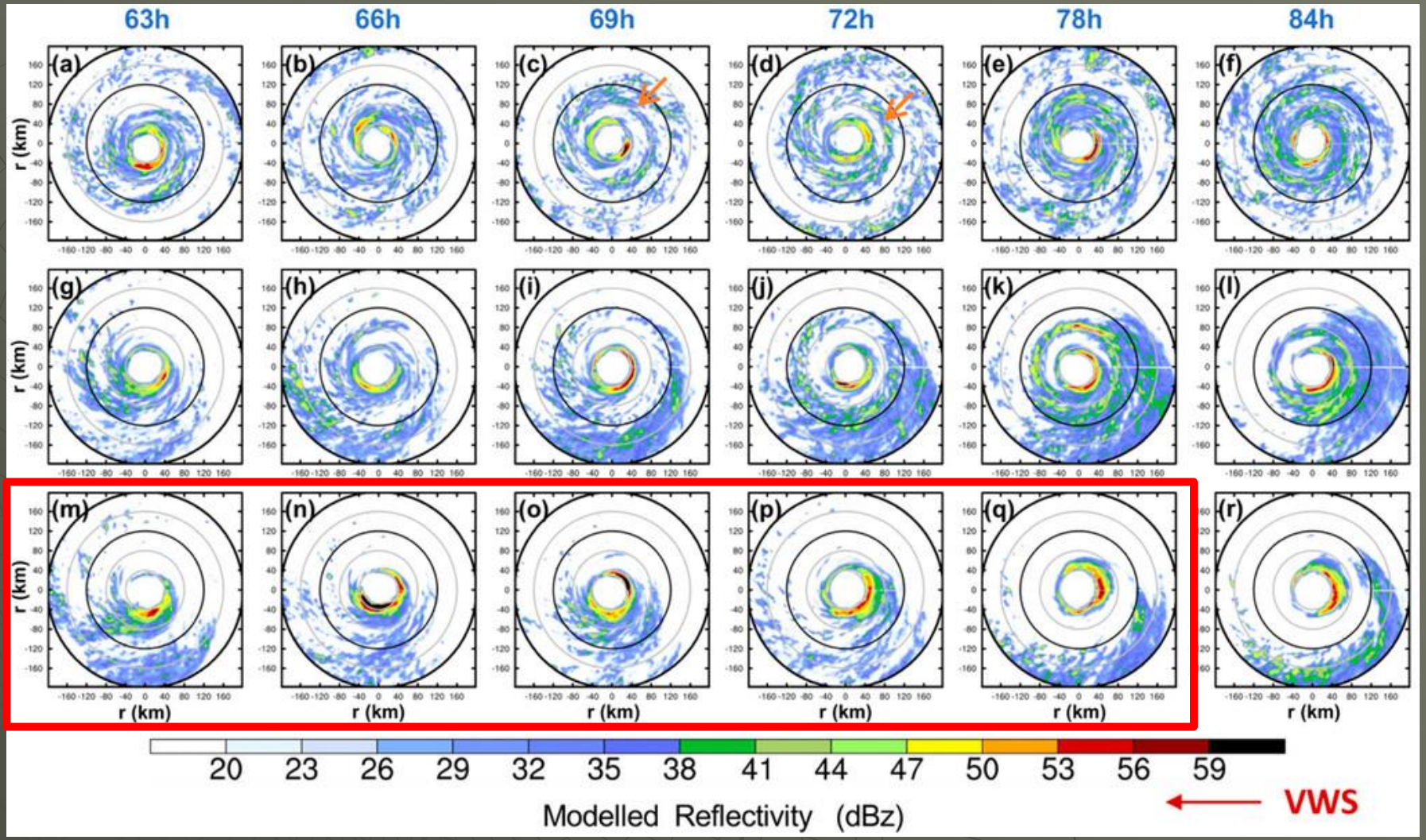

- Plan view of the modeled reflectivity (dBZ) at z = 3 km during 63–84 h. (a)–(f) CTRL, (g)–(l) SH08, and (m)–(r) SH12. Circles are shown at every 40 km from the storm center and the black circle highlights the 120 km radius. The red arrow indicates the shear direction. The orange arrows indicate the secondary convective ring in CTRL.

3. Overview and results —— b. Rainbands evolution cont.

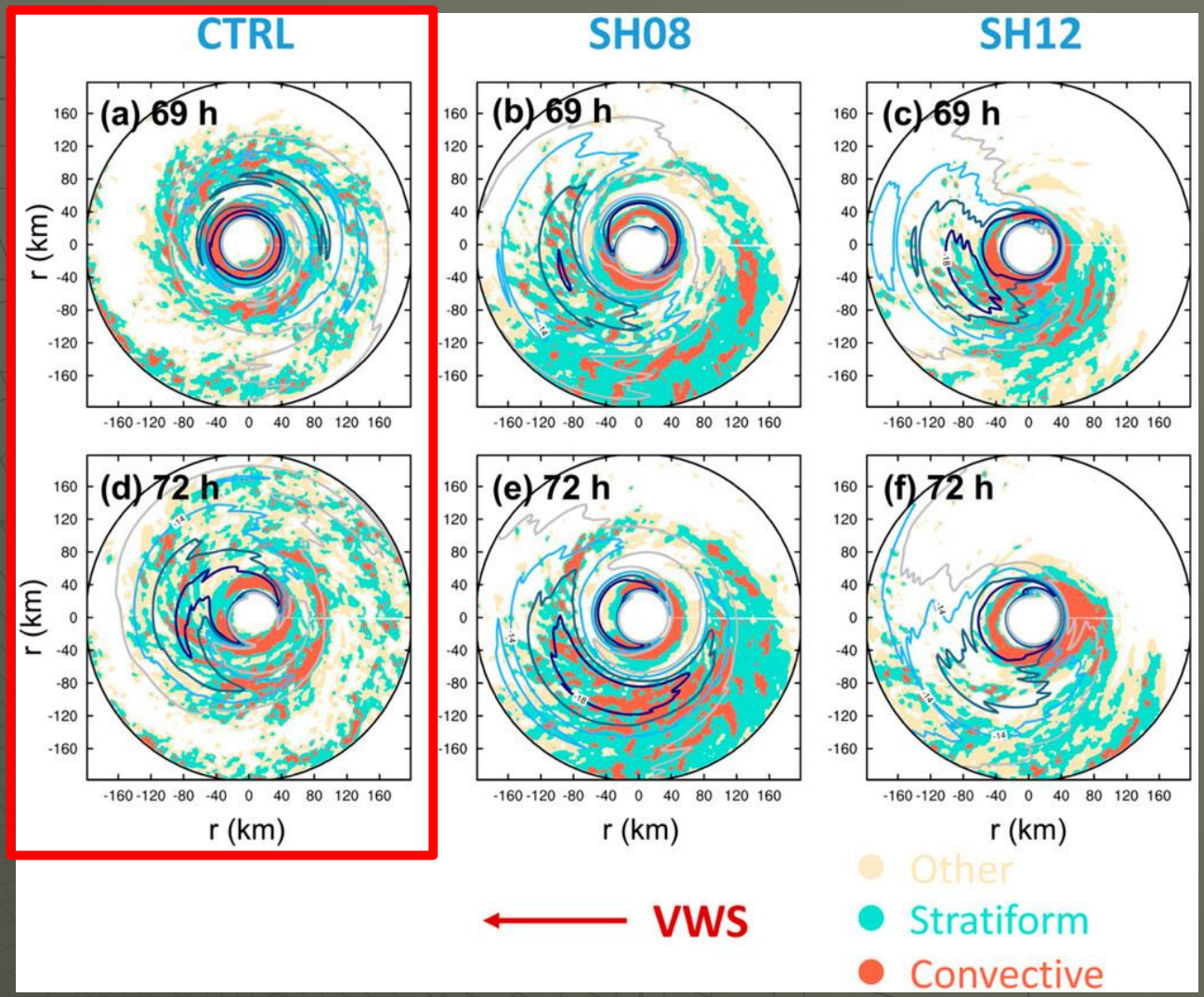

- (a)–(c) The convective–stratiform partitioning (shading) for (left) CTRL, (center) SH08, and (right) SH12 at 69 h following the algorithm of Rogers (2010). White region denotes "no rain." Contours represent radial velocity averaged (–12, –14, –16, and –18 m s^–1 with line colors from light to dark) at z = 600 m. (d)–(f) As in (a)–(c), but for 72 h.

3. Overview and results —— b. Rainbands evolution cont.

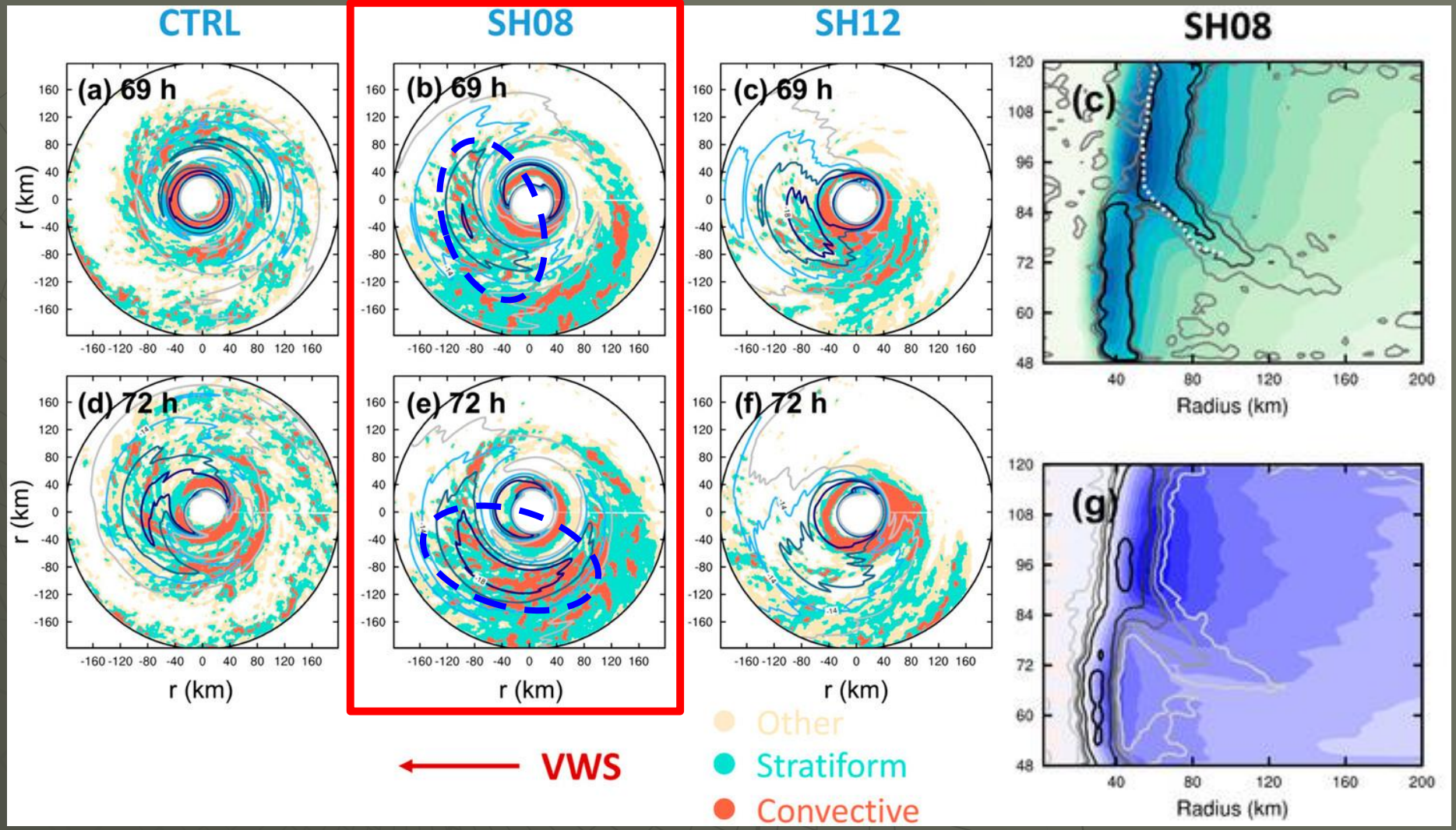

- (a)–(c) The convective–stratiform partitioning (shading) for (left) CTRL, (center) SH08, and (right) SH12 at 69 h following the algorithm of Rogers (2010). White region denotes "no rain." Contours represent radial velocity averaged (–12, –14, –16, and –18 m s^–1 with line colors from light to dark) at z = 600 m. (d)–(f) As in (a)–(c), but for 72 h.

3. Overview and results —— b. Rainbands evolution cont.

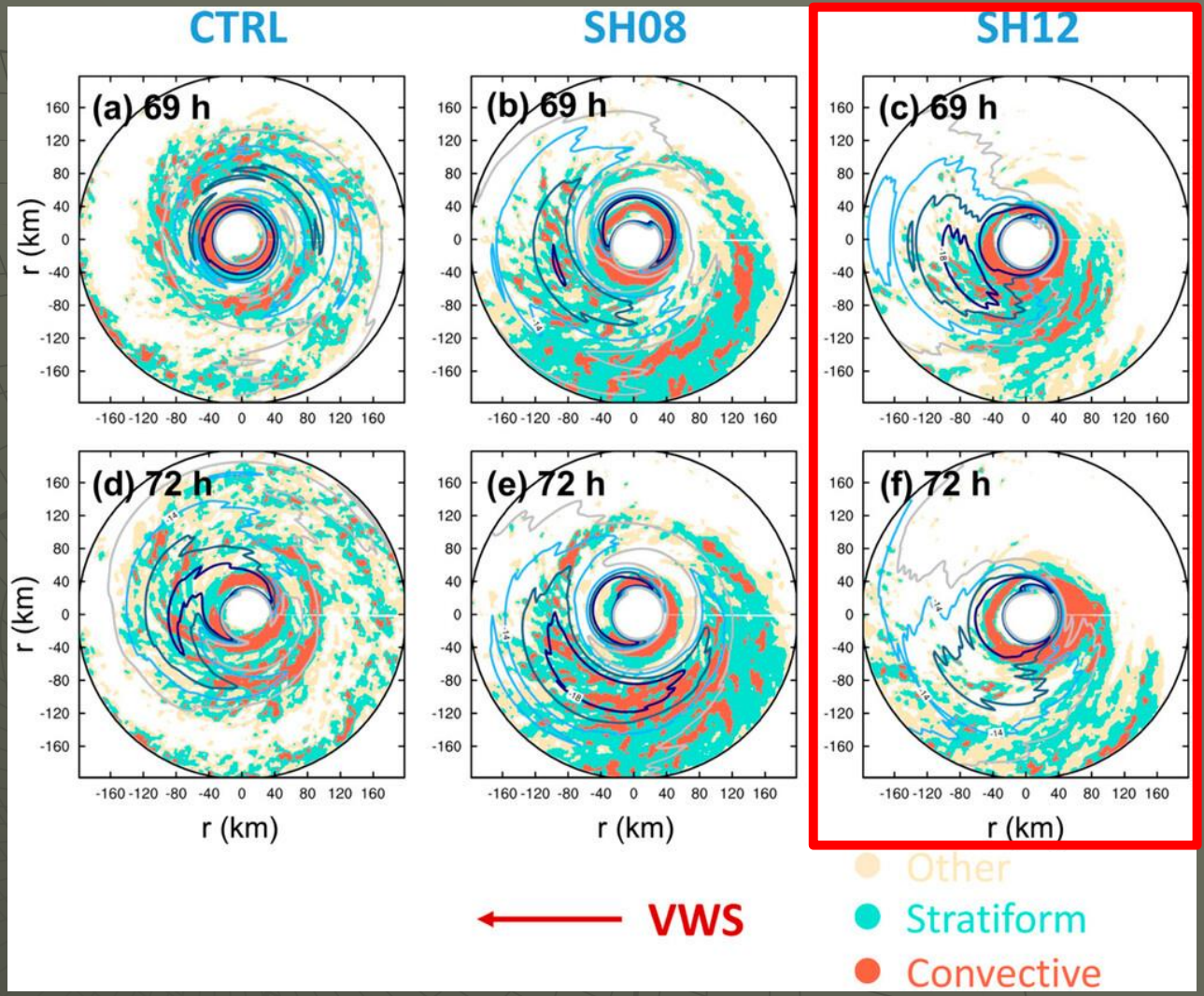

- (a)–(c) The convective–stratiform partitioning (shading) for (left) CTRL, (center) SH08, and (right) SH12 at 69 h following the algorithm of Rogers (2010). White region denotes "no rain." Contours represent radial velocity averaged (–12, –14, –16, and –18 m s^–1 with line colors from light to dark) at z = 600 m. (d)–(f) As in (a)–(c), but for 72 h.

3. Overview and results —— b. Rainbands evolution cont.

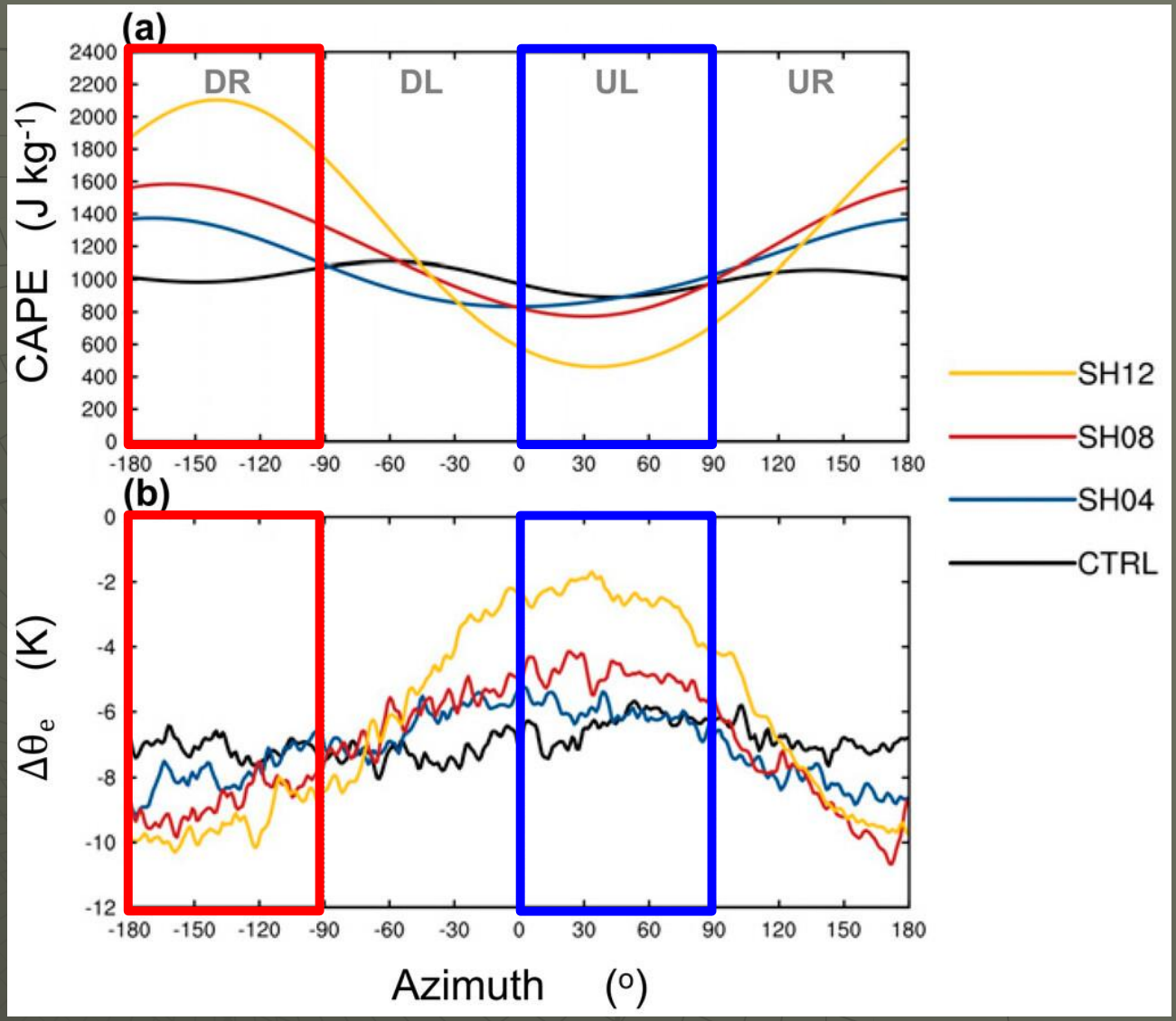

- The azimuthal distribution of the (a) CAPE (J kg^−1) and (b) Δθe (K, difference between z = 4 and 1 km, representing the low-level instability) average over 80–160 km radii during 66–72 h.

3. Overview and results —— b. Rainbands evolution cont.

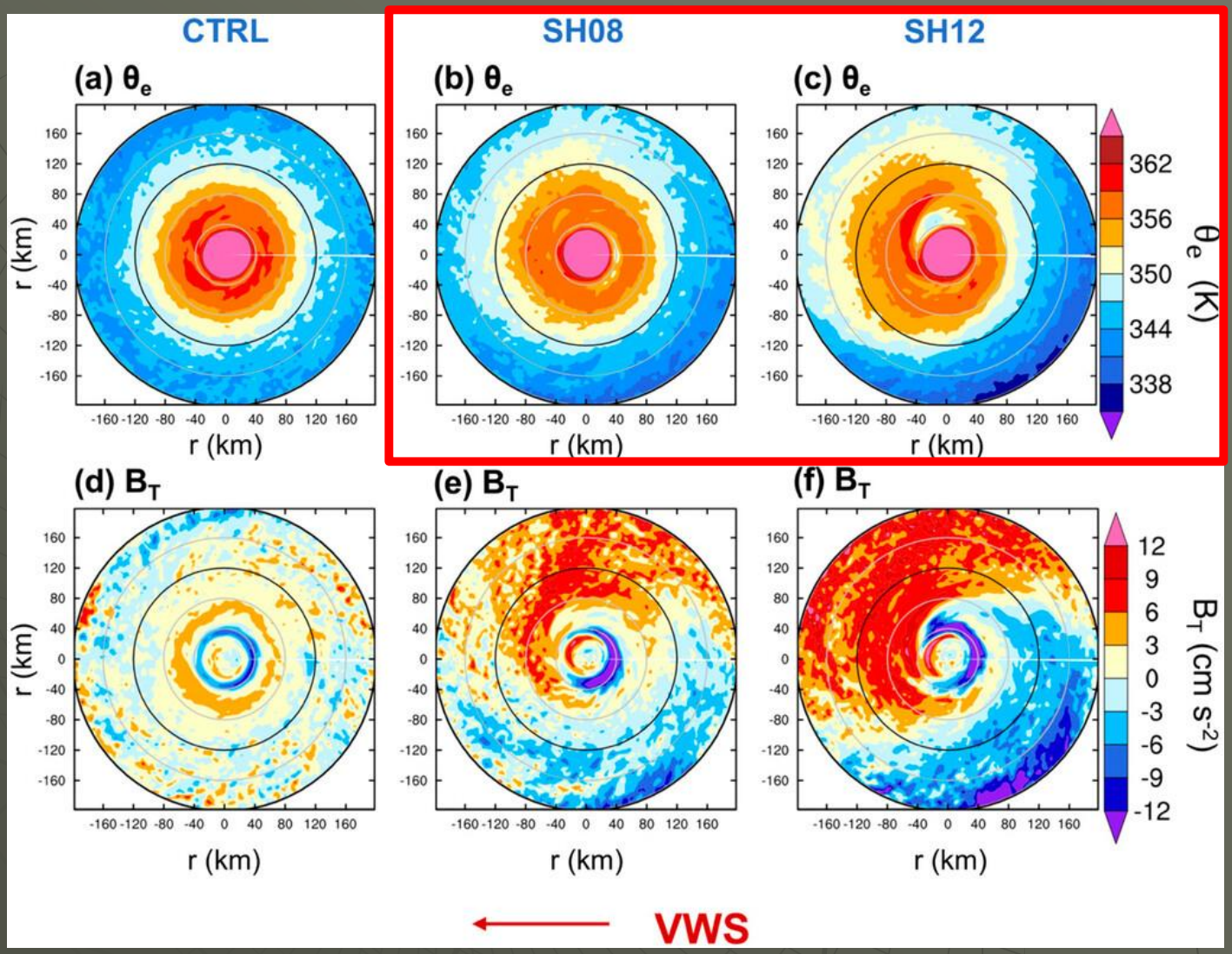

Eastin et al. (2012):

$$B_T = -g\frac{\theta'_e}{\overline{\theta}_e}$$

- Plan view of (a)–(c) θe (K) at z = 800 m and thermal buoyancy (cm s^−2) averaged between z = 0.8 and 1.2 km averaged over 66–72 h for (left) CTRL, (center) SH08, and (right) SH12.

3. Overview and results —— b. Rainbands evolution cont.

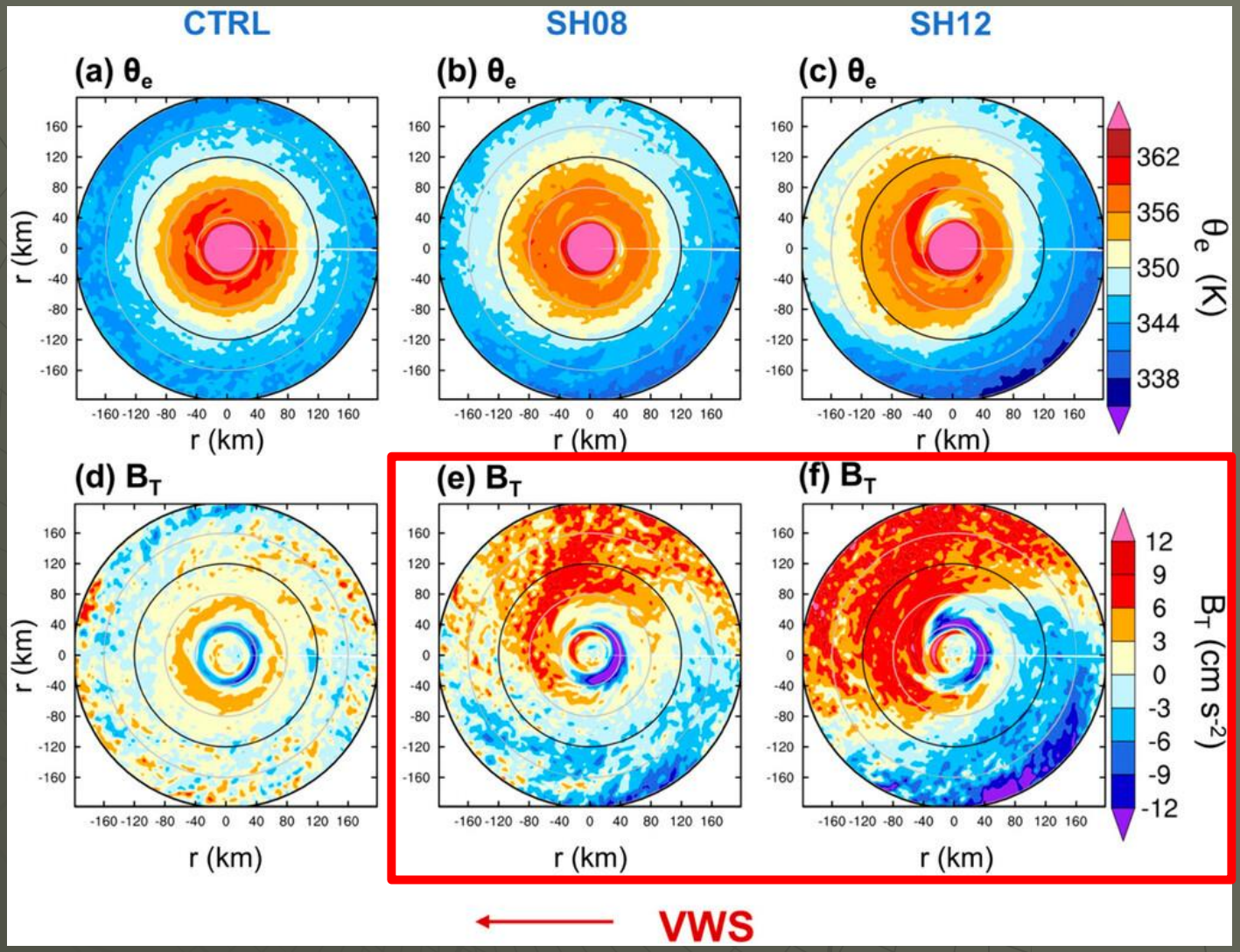

Eastin et al. (2012):

$$B_T = -g\frac{\theta'_e}{\overline{\theta}_e}$$

- Plan view of (a)–(c) θe (K) at z = 800 m and thermal buoyancy (cm s^−2) averaged between z = 0.8 and 1.2 km averaged over 66–72 h for (left) CTRL, (center) SH08, and (right) SH12.

4. ShearEvolution and BL response of rainbands at left of shear —— a. Rainbands structure and radial inflow

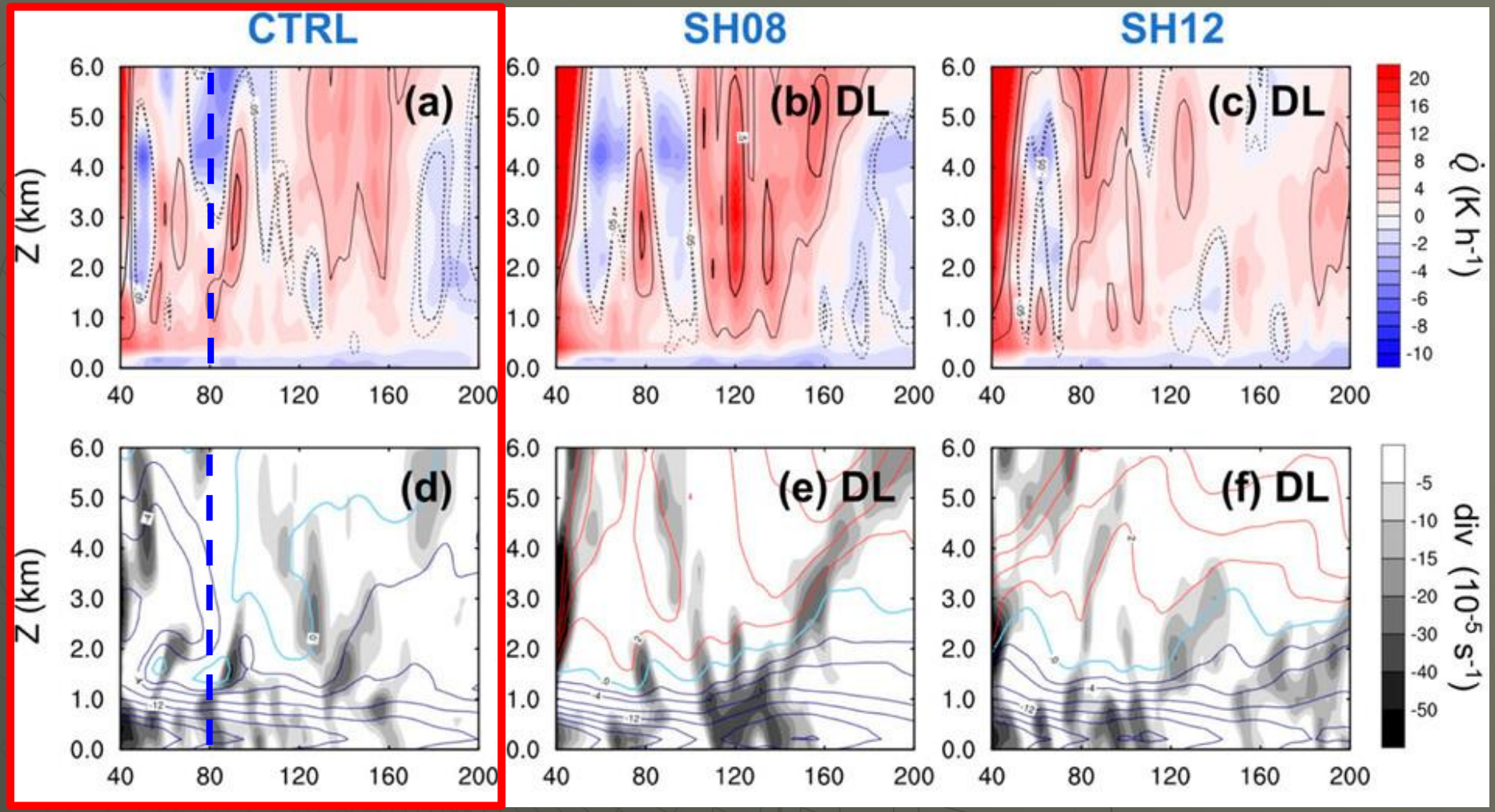

- The radius-height structure of (a)-(c) the diabatic heating rates (K h^-1) overlaid by vertical velocities (solid line at 0.25 and 0.5 m s^-1; dashed line at -0.025 and -0.05 m s^-1) and (d)-(f) radial divergence (10^-5 s^-1) overlaid by radial velocities (blue line at -2, -4, -8, -12, -16, and -20 m s^-1 and red line at 2, 4, and 6 m s^-1) averaged over the DL (southwest quadrant for CTRL) quadrant at 69 h.

4. ShearEvolution and BL response of rainbands at left of shear —— a. Rainbands structure and radial inflow cont.

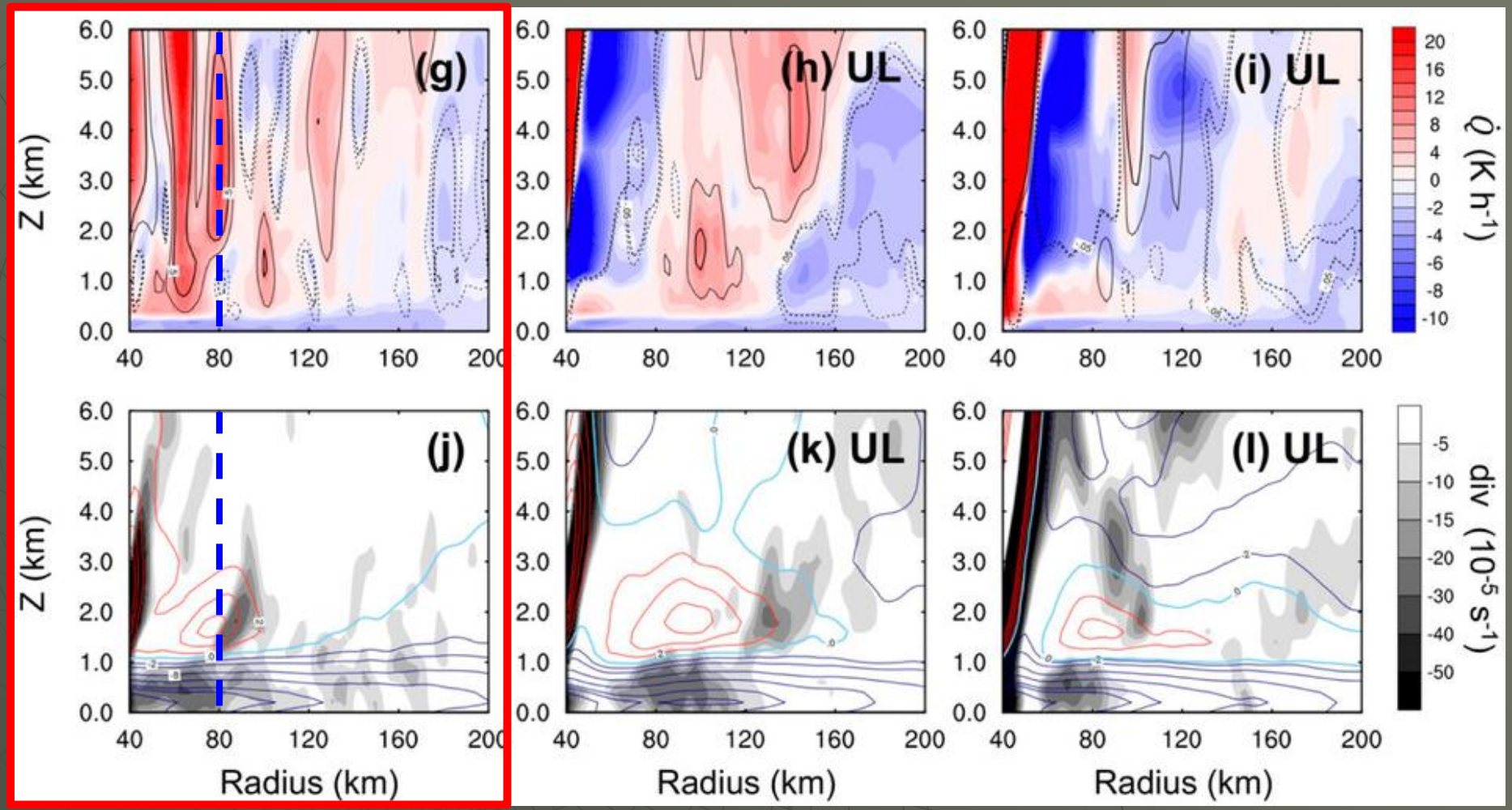

- (g)–(i) As in (a)–(c), but for UL and (j)–(l) as in (d)–(f), but for UL (southeast quadrant for CTRL). Columns show (left) CTRL, (center) SH08, and (right) SH12.

4. ShearEvolution and BL response of rainbands at left of shear —— a. Rainbands structure and radial inflow

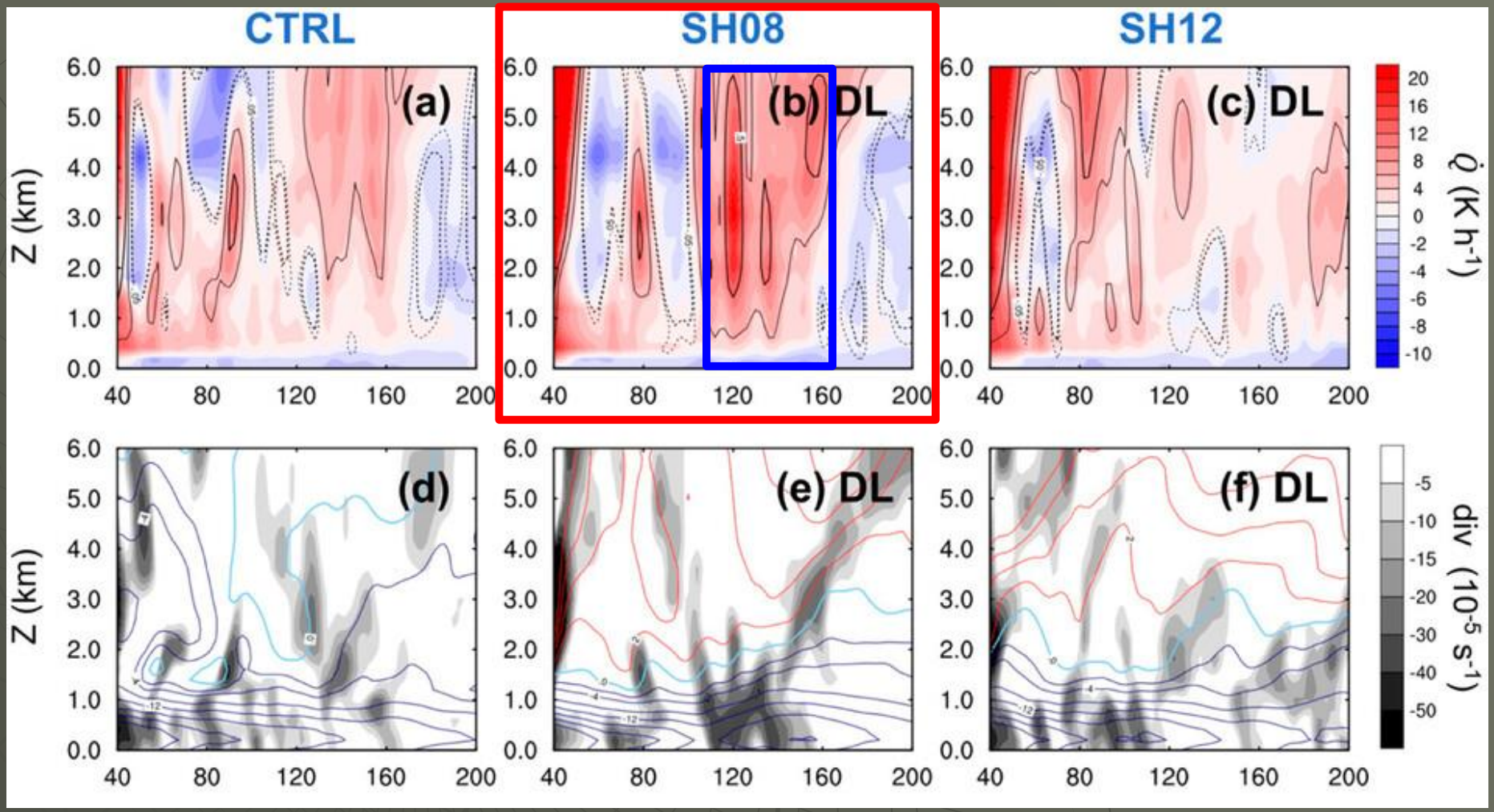

- The radius-height structure of (a)–(c) the diabatic heating rates (K h^−1) overlaid by vertical velocities (solid line at 0.25 and 0.5 m s^−1; dashed line at −0.025 and −0.05 m s^−1) and (d)–(f) radial divergence (10^−5 s^−1) overlaid by radial velocities (blue line at −2, −4, −8, −12, −16, and −20 m s^−1 and red line at 2, 4, and 6 m s^−1) averaged over the DL (southwest quadrant for CTRL) quadrant at 69 h.

4. ShearEvolution and BL response of rainbands at left of shear —— a. Rainbands structure and radial inflow cont.

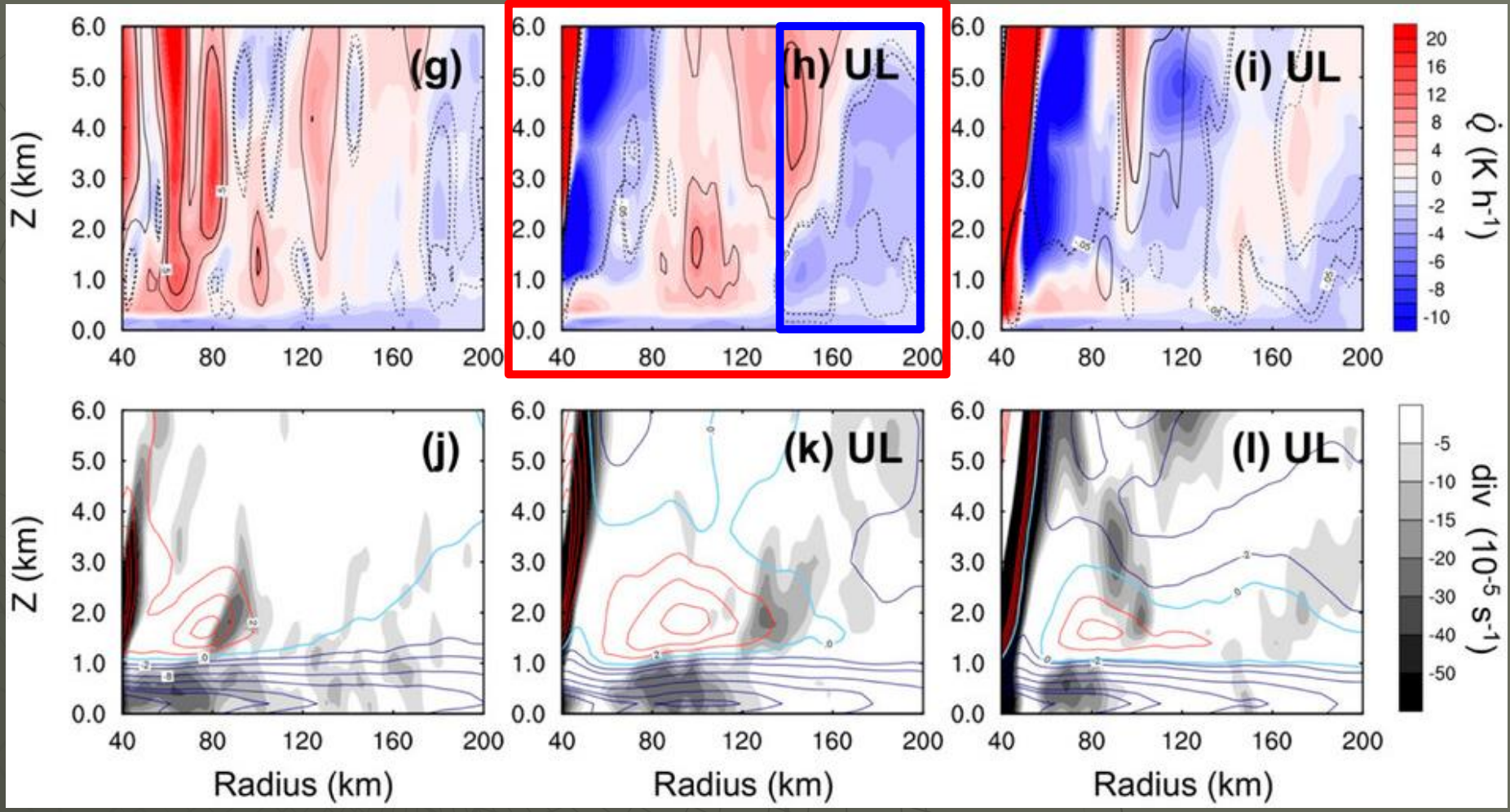

- (g)–(i) As in (a)–(c), but for UL and (j)–(l) as in (d)–(f), but for UL (southeast quadrant for CTRL). Columns show (left) CTRL, (center) SH08, and (right) SH12.

4. ShearEvolution and BL response of rainbands at left of shear —— a. Rainbands structure and radial inflow

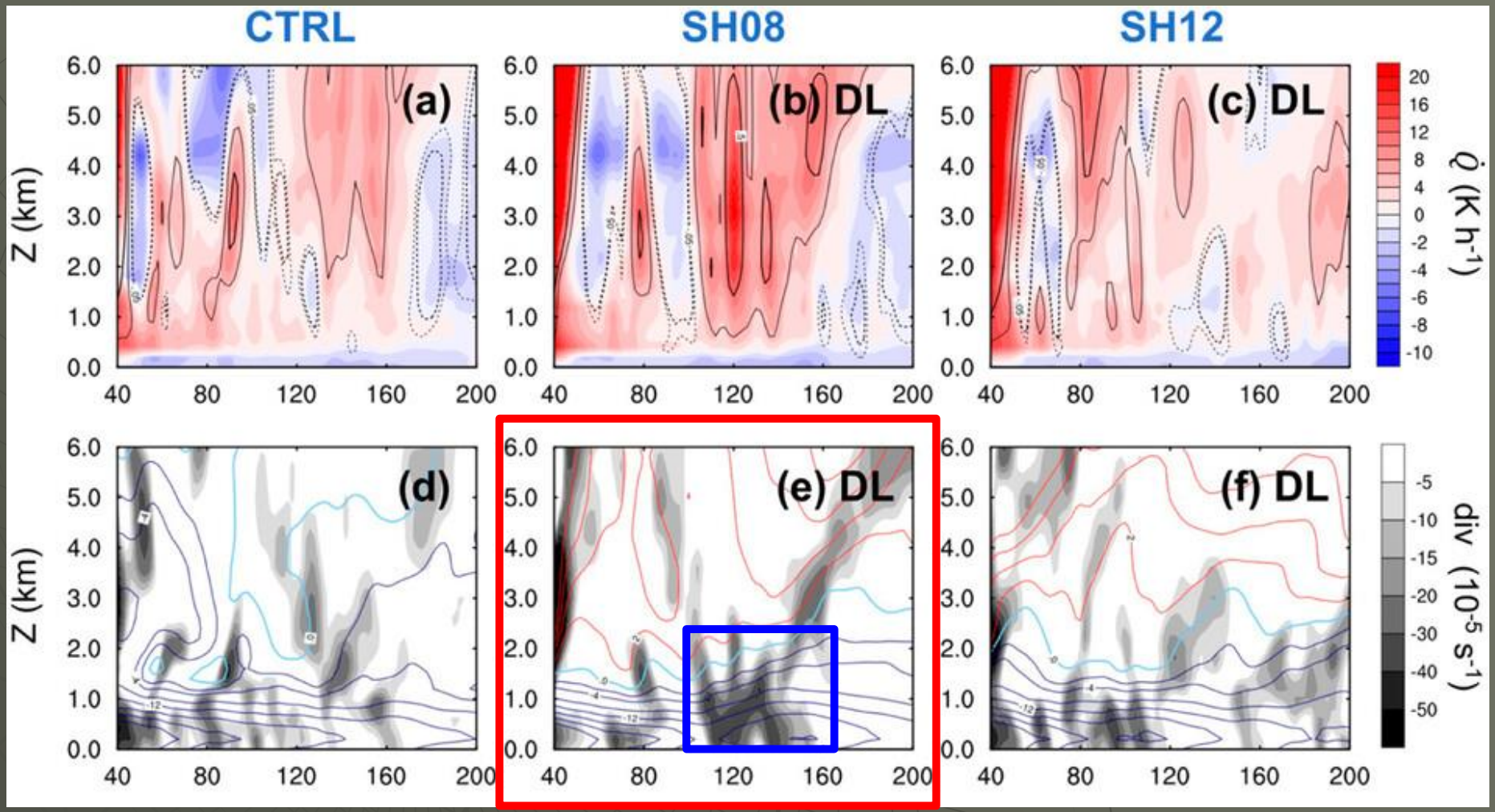

- The radius-height structure of (a)–(c) the diabatic heating rates (K h^−1) overlaid by vertical velocities (solid line at 0.25 and 0.5 m s^−1; dashed line at −0.025 and −0.05 m s^−1) and (d)–(f) radial divergence (10^−5 s^−1) overlaid by radial velocities (blue line at −2, −4, −8, −12, −16, and −20 m s^−1 and red line at 2, 4, and 6 m s^−1) averaged over the DL (southwest quadrant for CTRL) quadrant at 69 h.

4. ShearEvolution and BL response of rainbands at left of shear —— a. Rainbands structure and radial inflow cont.

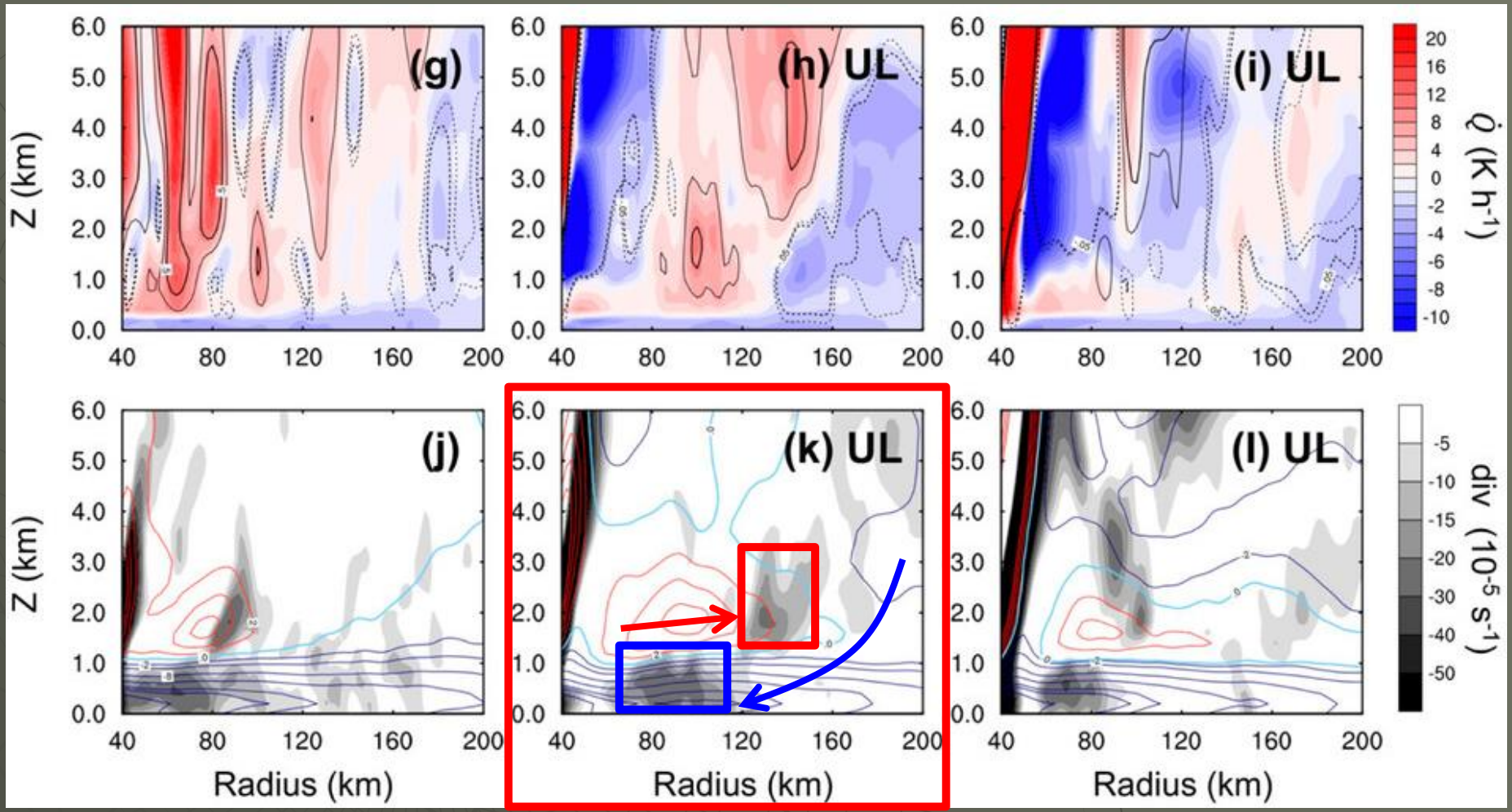

- (g)–(i) As in (a)–(c), but for UL and (j)–(l) as in (d)–(f), but for UL (southeast quadrant for CTRL). Columns show (left) CTRL, (center) SH08, and (right) SH12.

4. ShearEvolution and BL response of rainbands at left of shear —— a. Rainbands structure and radial inflow

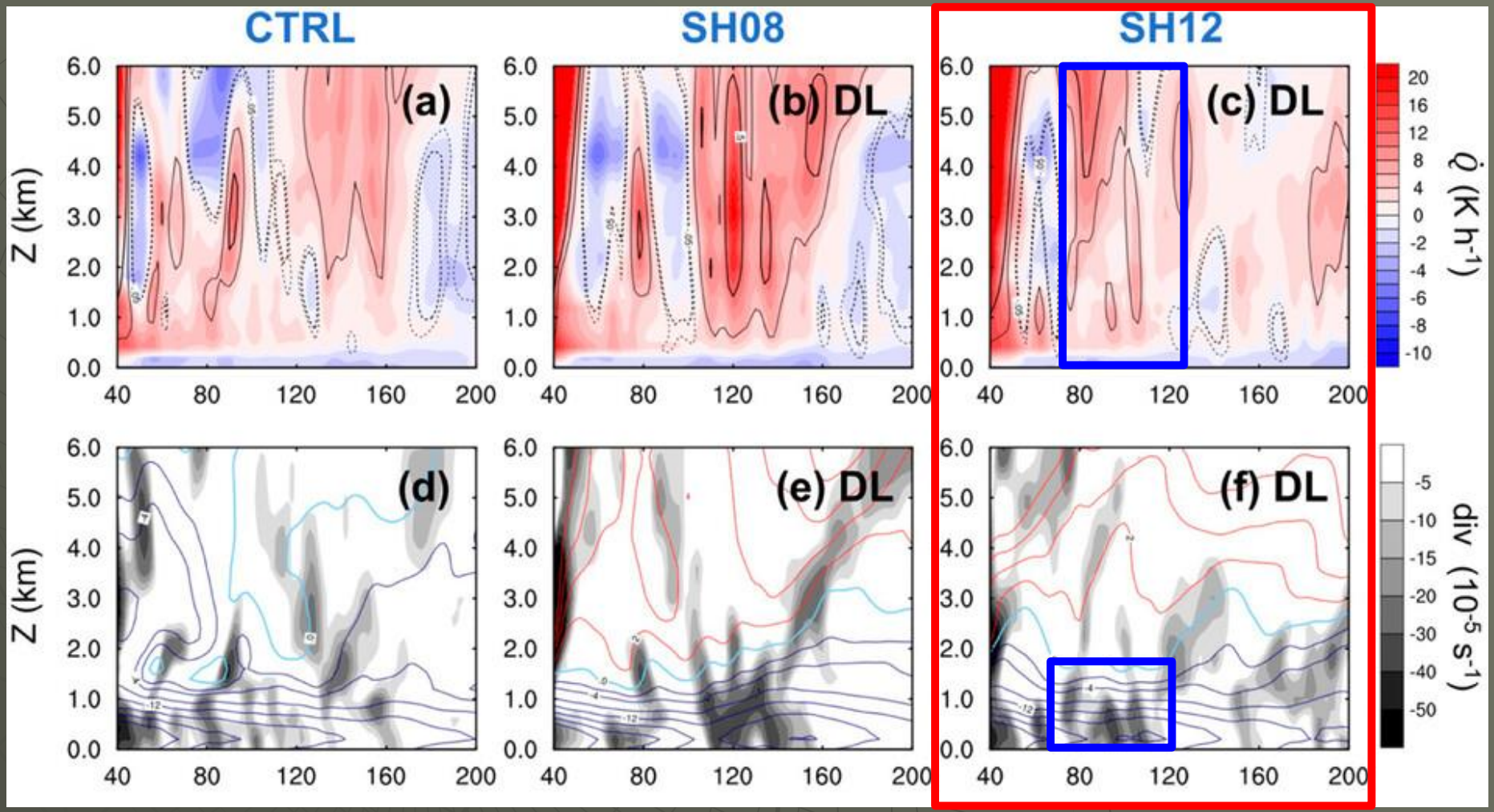

- The radius-height structure of (a)–(c) the diabatic heating rates (K h^−1) overlaid by vertical velocities (solid line at 0.25 and 0.5 m s^−1; dashed line at −0.025 and −0.05 m s^−1) and (d)–(f) radial divergence (10^−5 s^−1) overlaid by radial velocities (blue line at −2, −4, −8, −12, −16, and −20 m s^−1 and red line at 2, 4, and 6 m s^−1) averaged over the DL (southwest quadrant for CTRL) quadrant at 69 h.

4. ShearEvolution and BL response of rainbands at left of shear —— a. Rainbands structure and radial inflow cont.

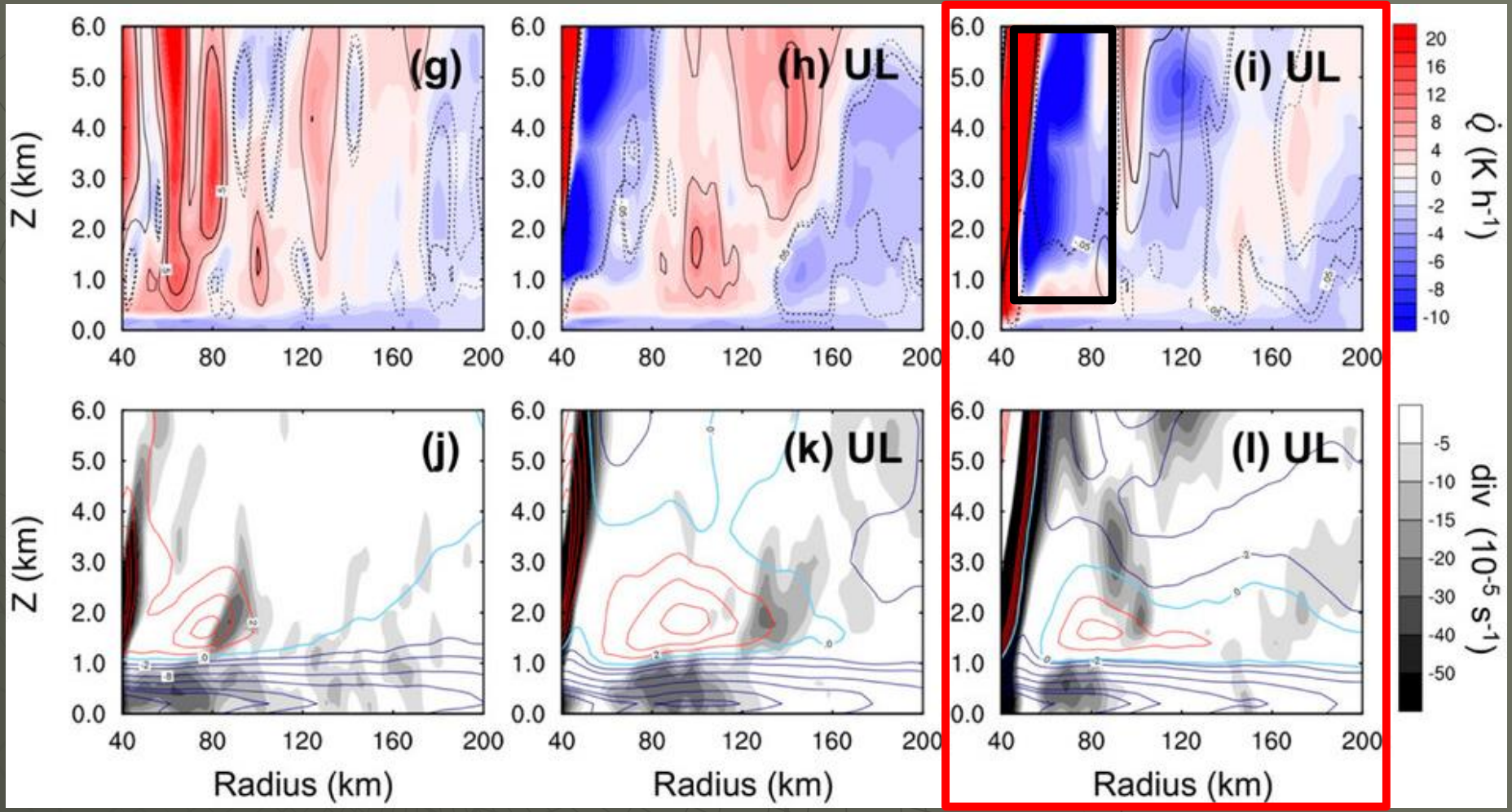

- (g)–(i) As in (a)–(c), but for UL and (j)–(l) as in (d)–(f), but for UL (southeast quadrant for CTRL). Columns show (left) CTRL, (center) SH08, and (right) SH12.

4. ShearEvolution and BL response of rainbands at left of shear —— b. Enhancement convection in the UL

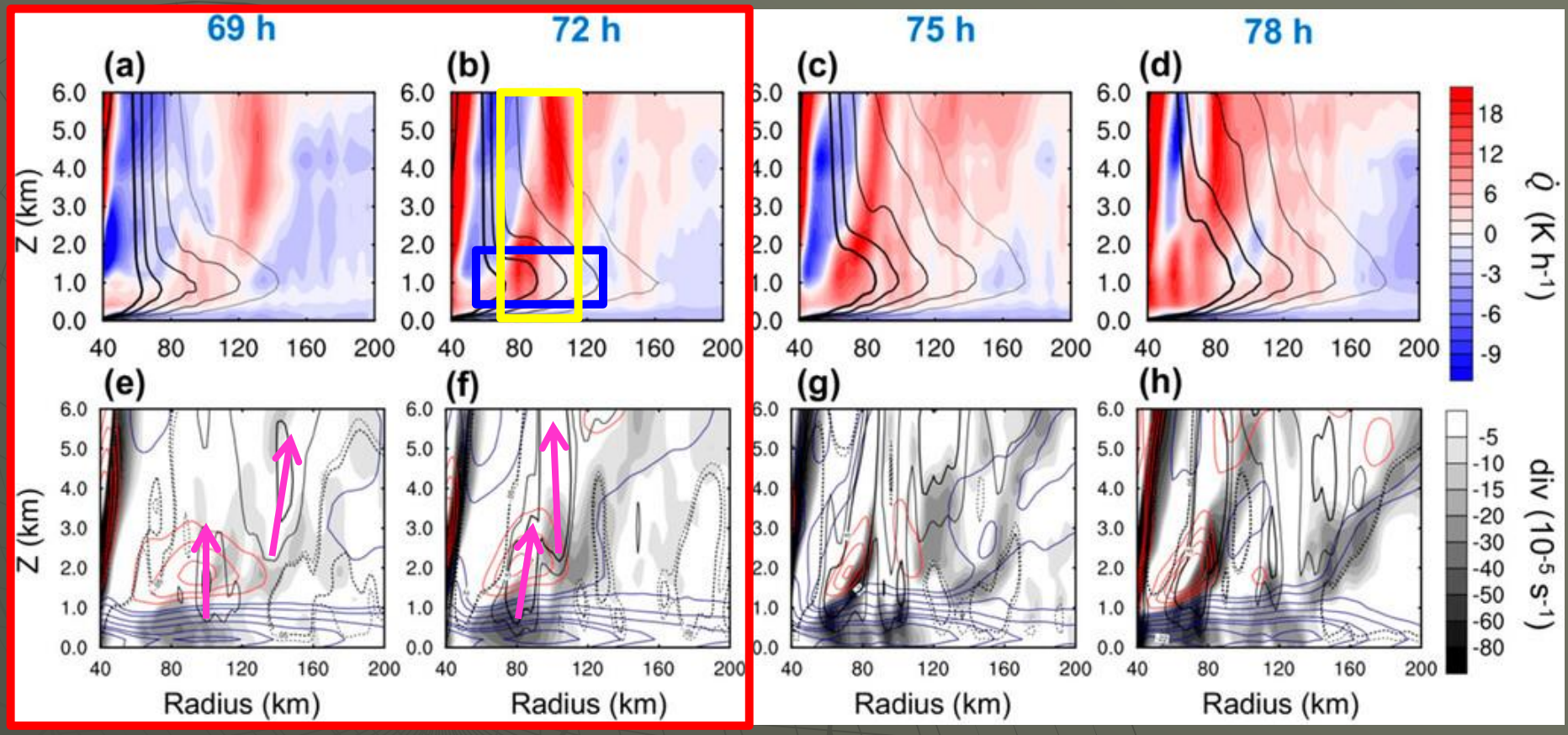

- Radius-height structures averaged over the UL of SH08 during 69–78 h with 3 h interval. (a)–(d) Diabatic heating rates (K h^−1) overlaid by tangential velocities (at every 5 m s^−1 from 45 to 65 m s^−1). (e)–(h) Shading represents radial divergence (10^−5 s^−1). Radial velocities are shown in blue (−2, −4, −8, −12, −16, −18, and −22 m s^−1) and red contours (2, 4, 6, and 8 m s^−1). Vertical velocities are shown in black contours (solid line at 0.25 and 0.5 m s^−1; dashed line at −0.025 and −0.05 m s^−1).

4. ShearEvolution and BL response of rainbands at left of shear —— b. Enhancement convection in the UL cont.

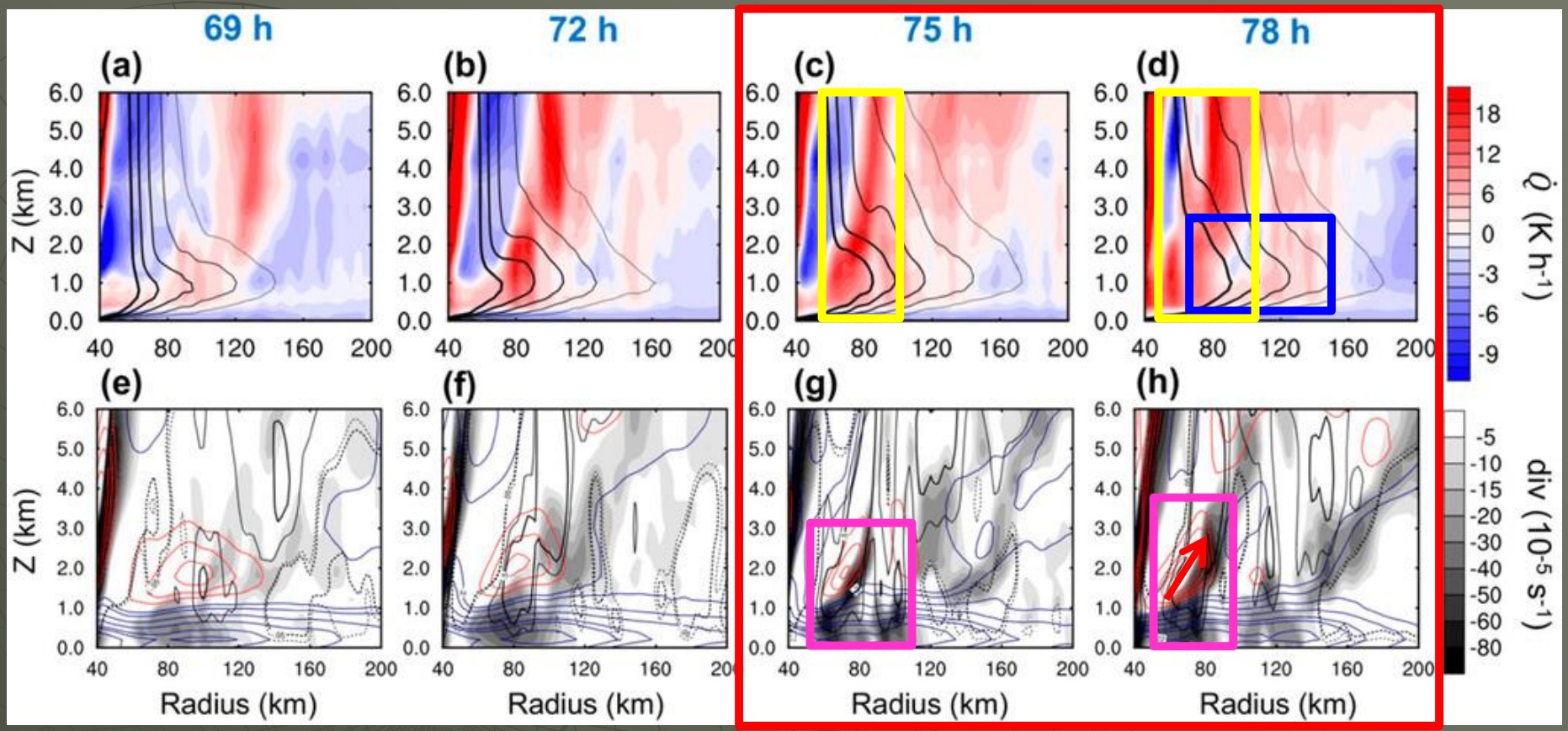

- Radius-height structures averaged over the UL of SH08 during 69–78 h with 3 h interval. (a)–(d) Diabatic heating rates (K h^−1) overlaid by tangential velocities (at every 5 m s^−1 from 45 to 65 m s^−1). (e)–(h) Shading represents radial divergence (10^−5 s^−1). Radial velocities are shown in blue (−2, −4, −8, −12, −16, −18, and −22 m s^−1) and red contours (2, 4, 6, and 8 m s^−1). Vertical velocities are shown in black contours (solid line at 0.25 and 0.5 m s^−1; dashed line at −0.025 and −0.05 m s^−1).

5. Convection initiation at UR

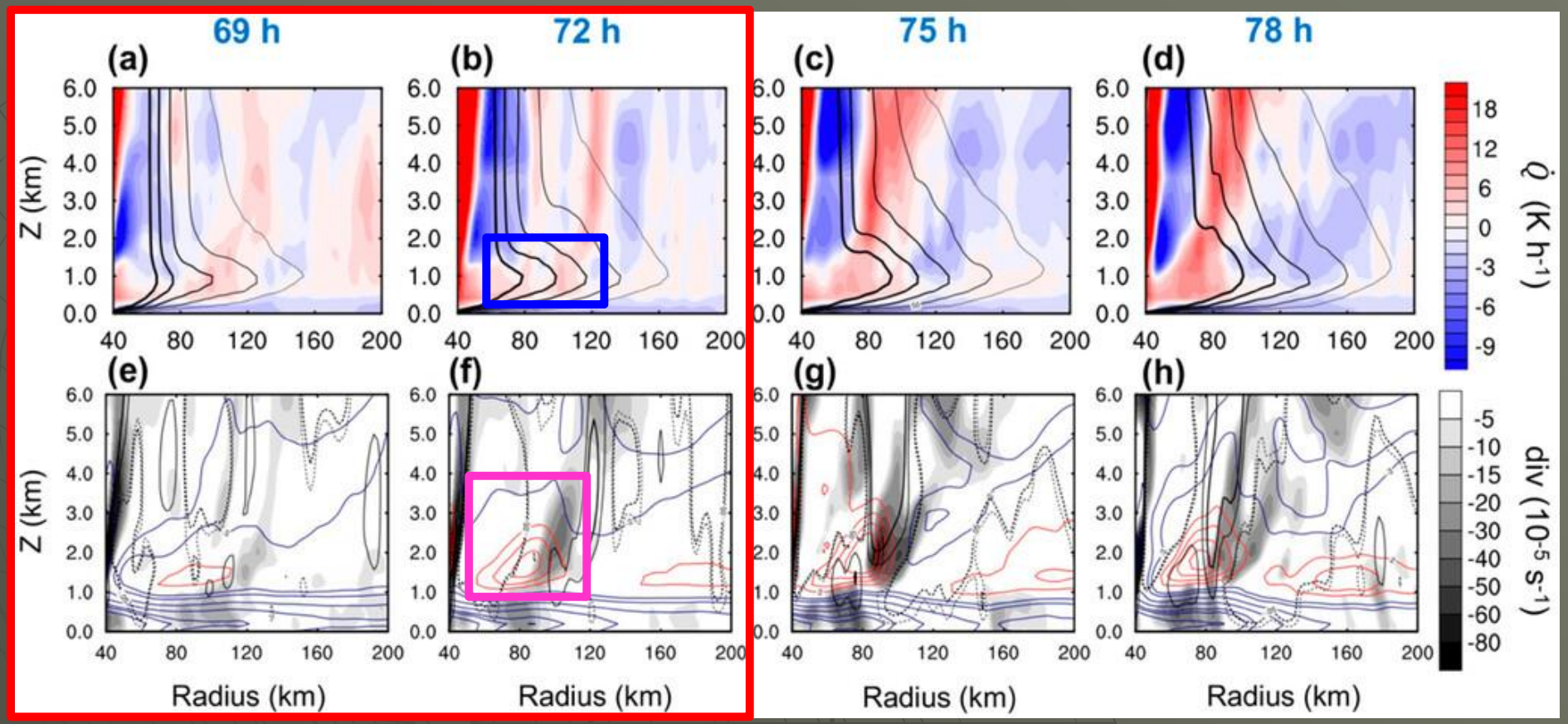

- Radius–height structures averaged over the UR of SH08 during 69–78 h with 3 h interval. (a)–(d) Diabatic heating rates (K h^−1) overlaid by tangential velocities (at every 5 m s^−1 from 45 to 65 m s^−1). (e)–(h) Shading represents radial divergence (10^−5 s^−1). Radial velocities are shown in blue (−2, −4, −8, −12, −16, −18, and −22 m s^−1) and red contours (2, 4, 6, and 8 m s^−1). Vertical velocities are shown in black contours (solid line at 0.25 and 0.5 m s^−1; dashed line at −0.025 and −0.05 m s^−1).

5. Convection initiation at UR cont.

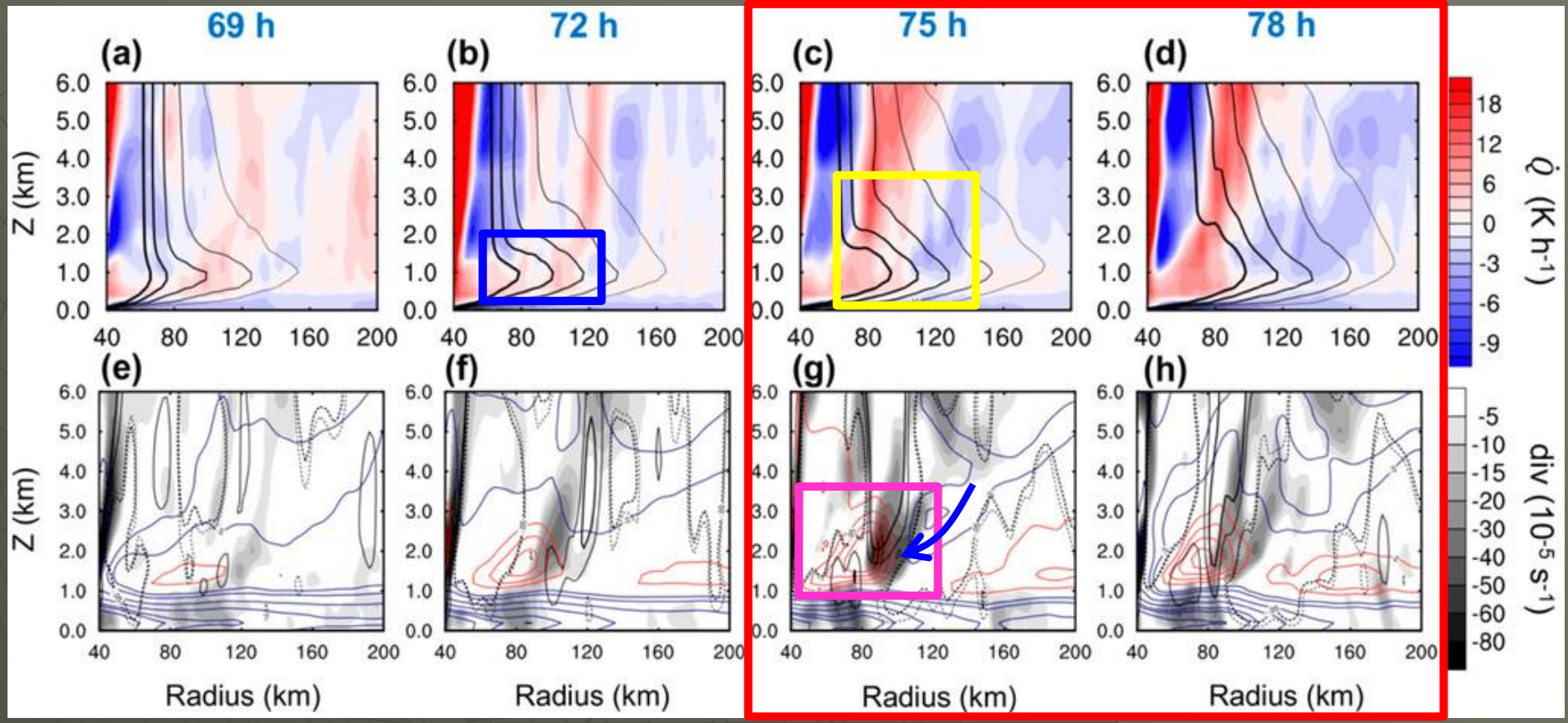

- Radius–height structures averaged over the UR of SH08 during 69–78 h with 3 h interval. (a)–(d) Diabatic heating rates (K h^−1) overlaid by tangential velocities (at every 5 m s^−1 from 45 to 65 m s^−1). (e)–(h) Shading represents radial divergence (10^−5 s^−1). Radial velocities are shown in blue (−2, −4, −8, −12, −16, −18, and −22 m s^−1) and red contours (2, 4, 6, and 8 m s^−1). Vertical velocities are shown in black contours (solid line at 0.25 and 0.5 m s^−1; dashed line at −0.025 and −0.05 m s^−1).

5. Convection initiation at UR cont.

- The agradient force (AGF), gradient wind balance, and agradient wind are given as follows:

$$\mathrm{AGF} = fv + \frac{v^2}{r} - \frac{1}{\rho}\frac{\partial P}{\partial r}$$

$$fv_g + \frac{v_g^2}{r} - \frac{1}{\rho}\frac{\partial P}{\partial r} = 0$$

$$v_a = v - v_g$$

- where v stands for total storm-relative tangential velocities, vg indicates gradient wind, and va indicates agradient wind; f, ρ, and p are Coriolis parameter, air density, and pressure, respectively.

5. Convection initiation at UR cont.

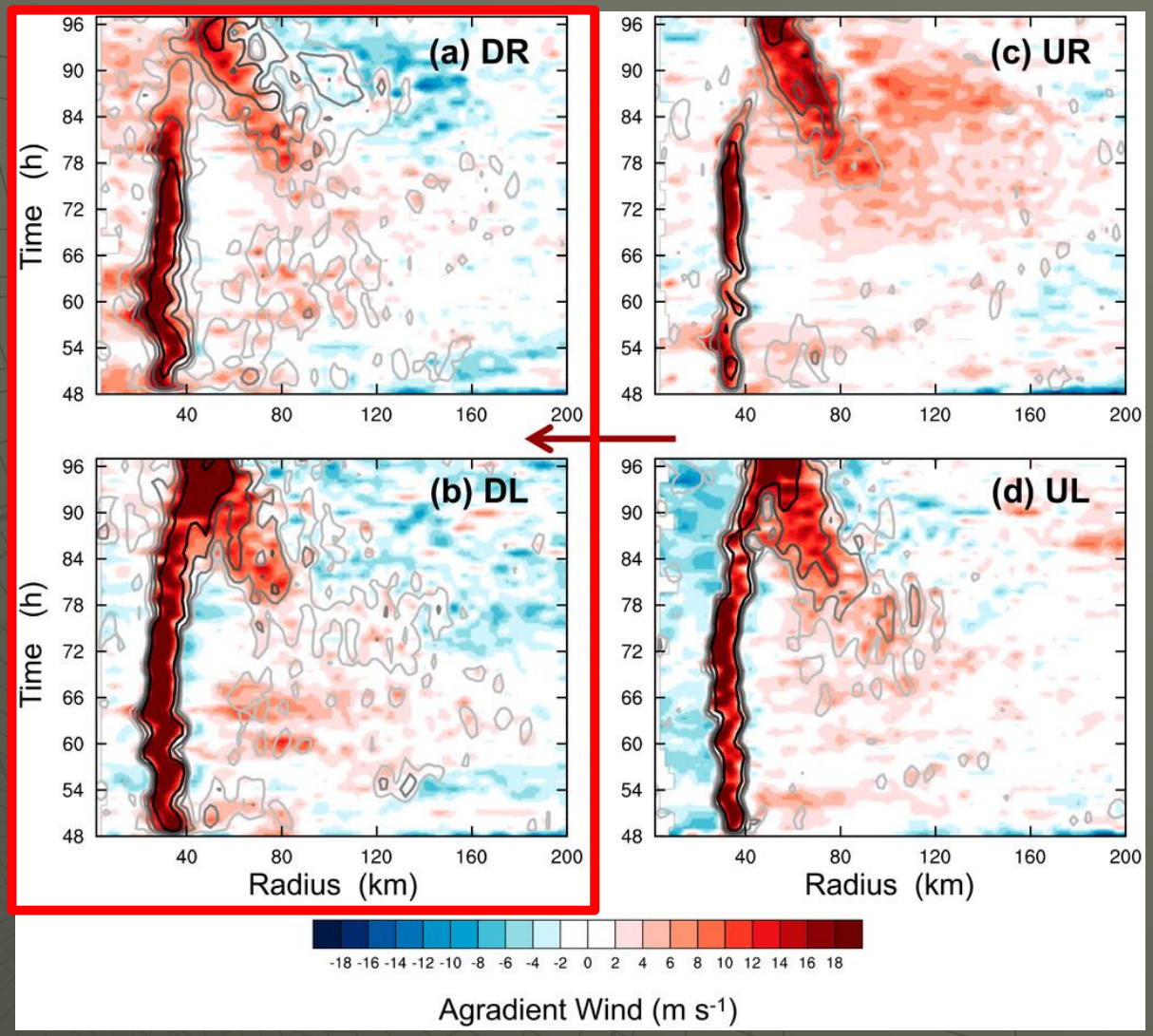

- Quadrant-averaged time–radius evolution of the agradient wind average between z = 0.6 and 1.0 km (m s^−1, shading) overlaid with the vertical velocity at z = 1 km (m s^−1, contours at 0.2, 0.5, 1.0, and 2.0 m s^−1) in SH08. The red arrow between the rows indicates the shear direction.

5. Convection initiation at UR cont.

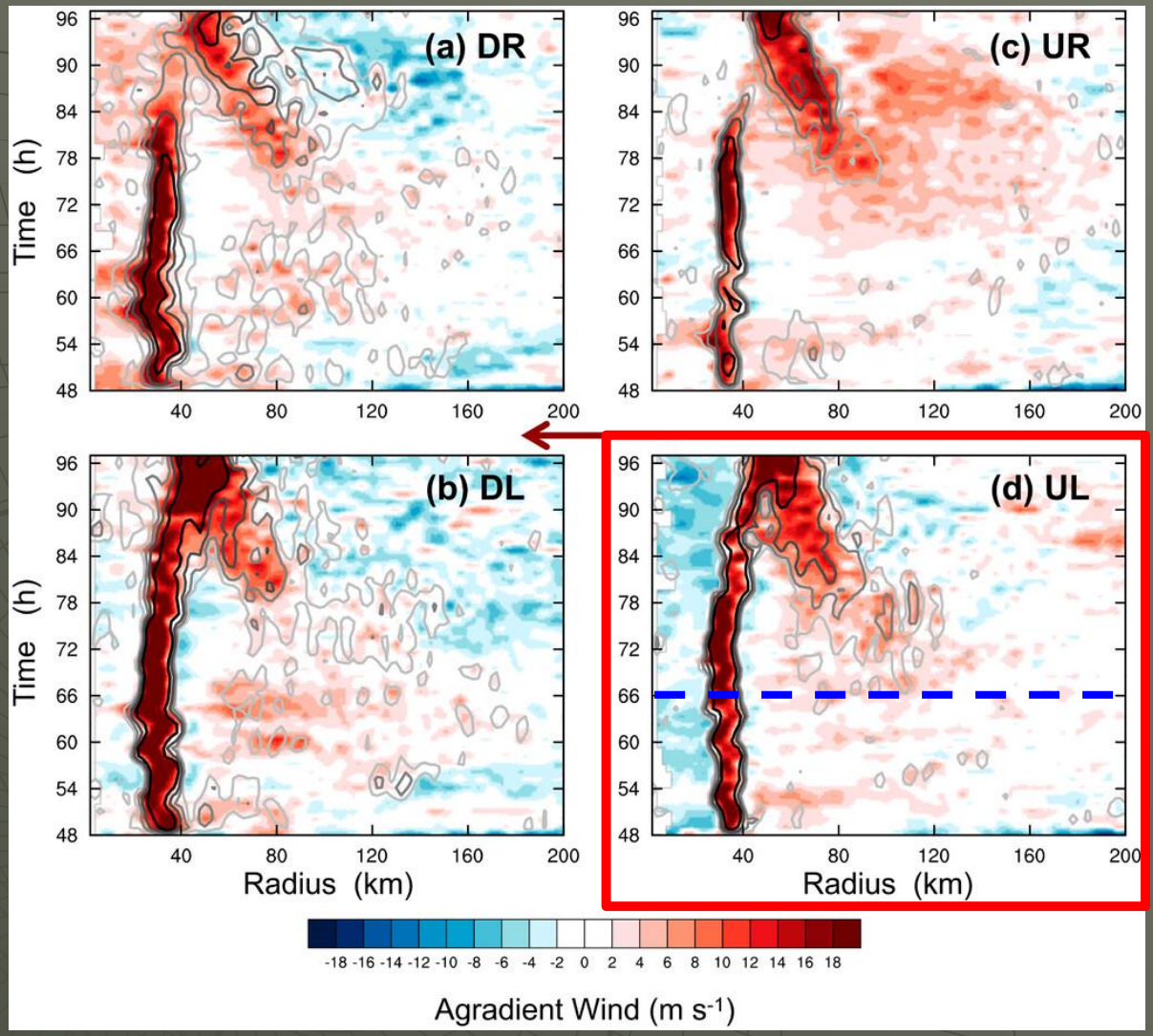

- Quadrant-averaged time–radius evolution of the agradient wind average between z = 0.6 and 1.0 km (m s^−1, shading) overlaid with the vertical velocity at z = 1 km (m s^−1, contours at 0.2, 0.5, 1.0, and 2.0 m s^−1) in SH08. The red arrow between the rows indicates the shear direction.

5. Convection initiation at UR cont.

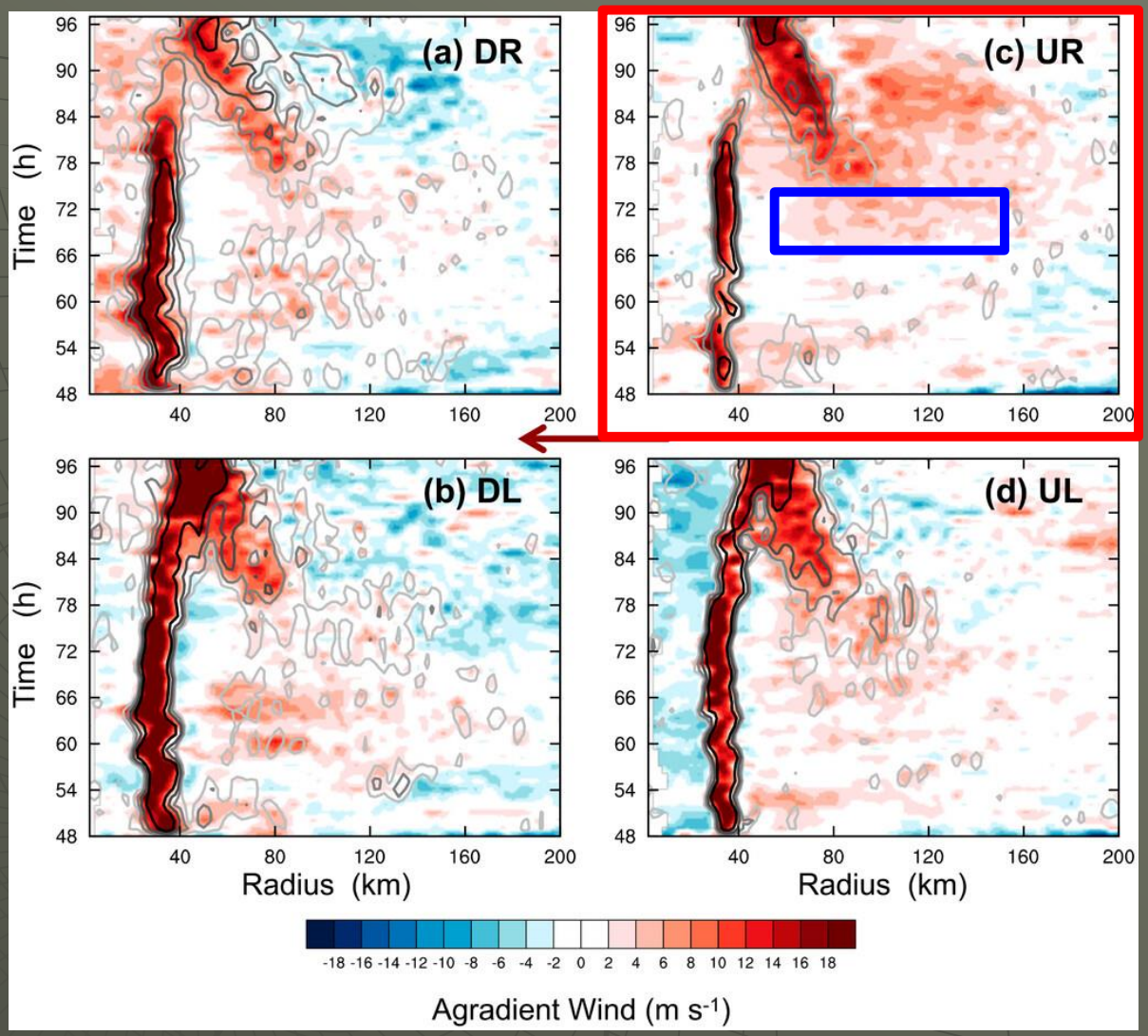

- Quadrant-averaged time–radius evolution of the agradient wind average between z = 0.6 and 1.0 km (m s^−1, shading) overlaid with the vertical velocity at z = 1 km (m s^−1, contours at 0.2, 0.5, 1.0, and 2.0 m s^−1) in SH08. The red arrow between the rows indicates the shear direction.

5. Convection initiation at UR cont.

- The governing equation of tangential wind tendency in cylindrical coordinates is given as follows:

$$\frac{\partial v}{\partial t} = -u(f+\zeta) - v\frac{\partial v}{r\partial \lambda} - w\frac{\partial v}{\partial z} - \frac{1}{\rho}\frac{\partial p}{r\partial \lambda} + F_{\lambda}$$

- where u, υ, and w are the radial, tangential, and vertical components of the storm-relative velocities, respectively; r, λ, and z indicate radial, tangential, and vertical direction of cylindrical coordinates, respectively.

- The terms on the right-hand side are radial advection, tangential advection and vertical advection, tangential pressure gradient force, and diffusion term, respectively.

5. Convection initiation at UR cont.

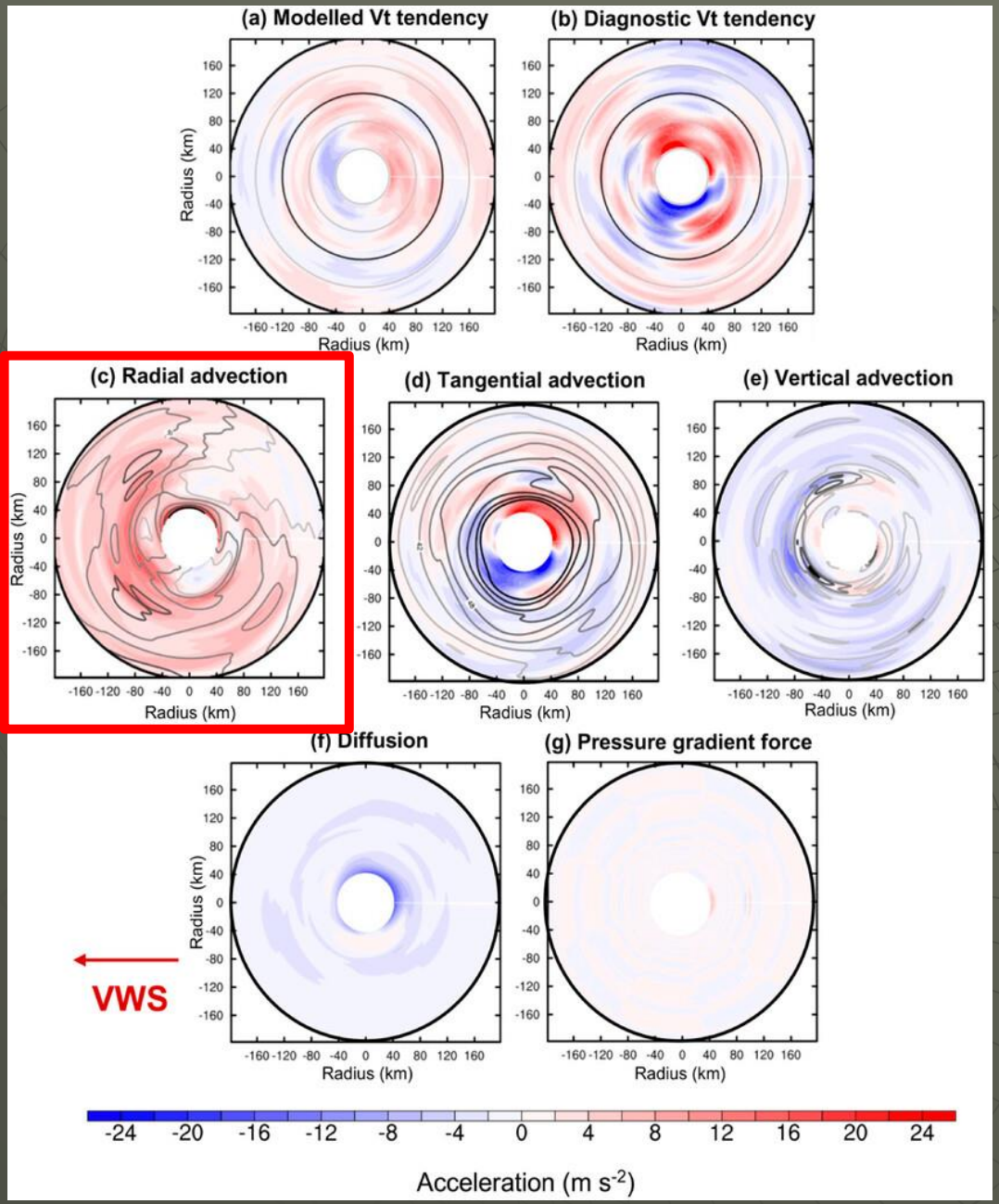

- Plan view of tangential wind budget at z = 1 km during 69–72 h in SH08: (a) modeled tangential wind tendency (m s^–1 h^–1), (b) calculated tangential wind speed tendency (m s^–1 h^–1), (c) radial advection term (m s^–1 h^–1, shading) and mean radial velocities (contours from 2 to 8 at 2 m s^–1 interval) during 69–72 h, (d) tendency of tangential advection (m s^–1 h^–1, shading) and mean tangential wind speed (contours from 39 to 60 at 3 m s^–1 interval), (e) vertical advection term (m s^–1 h^–1, shading) and mean vertical velocities (contours from 0.25 to 1 at 0.25 m s^–1 interval), (f) diffusion term (m s^–1 h^–1), and (g) tangential pressure gradient force (m s^–1 h^–1). The red arrow in the bottom left denotes the shear direction. Values within 40 km radius are omitted.

5. Convection initiation at UR cont.

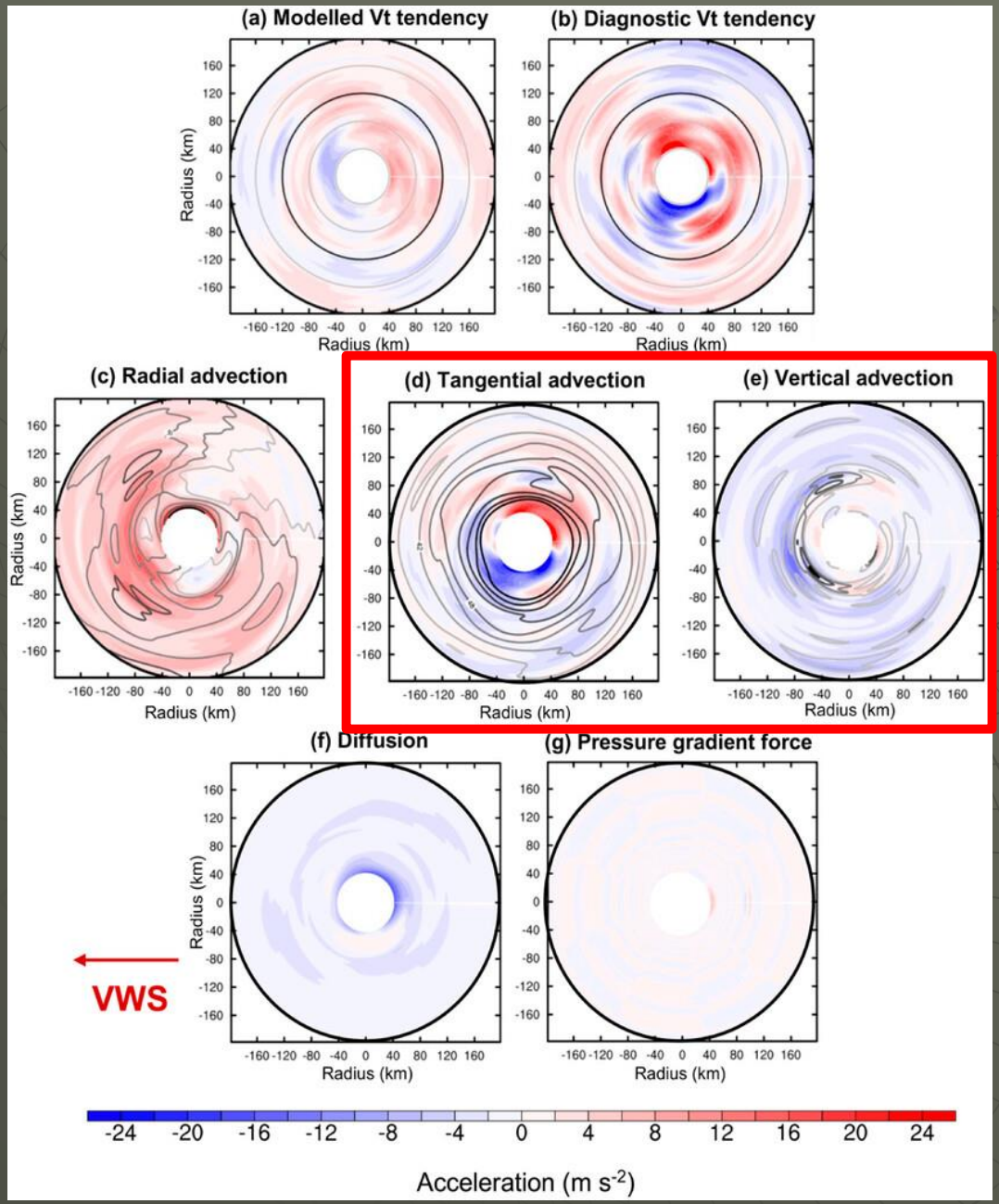

- Plan view of tangential wind budget at z = 1 km during 69–72 h in SH08: (a) modeled tangential wind tendency (m s^–1 h^–1), (b) calculated tangential wind speed tendency (m s^–1 h^–1), (c) radial advection term (m s^–1 h^–1, shading) and mean radial velocities (contours from 2 to 8 at 2 m s^–1 interval) during 69–72 h, (d) tendency of tangential advection (m s^–1 h^–1, shading) and mean tangential wind speed (contours from 39 to 60 at 3 m s^–1 interval), (e) vertical advection term (m s^–1 h^–1, shading) and mean vertical velocities (contours from 0.25 to 1 at 0.25 m s^–1 interval), (f) diffusion term (m s^–1 h^–1), and (g) tangential pressure gradient force (m s^–1 h^–1). The red arrow in the bottom left denotes the shear direction. Values within 40 km radius are omitted.

5. Convection initiation at UR cont.

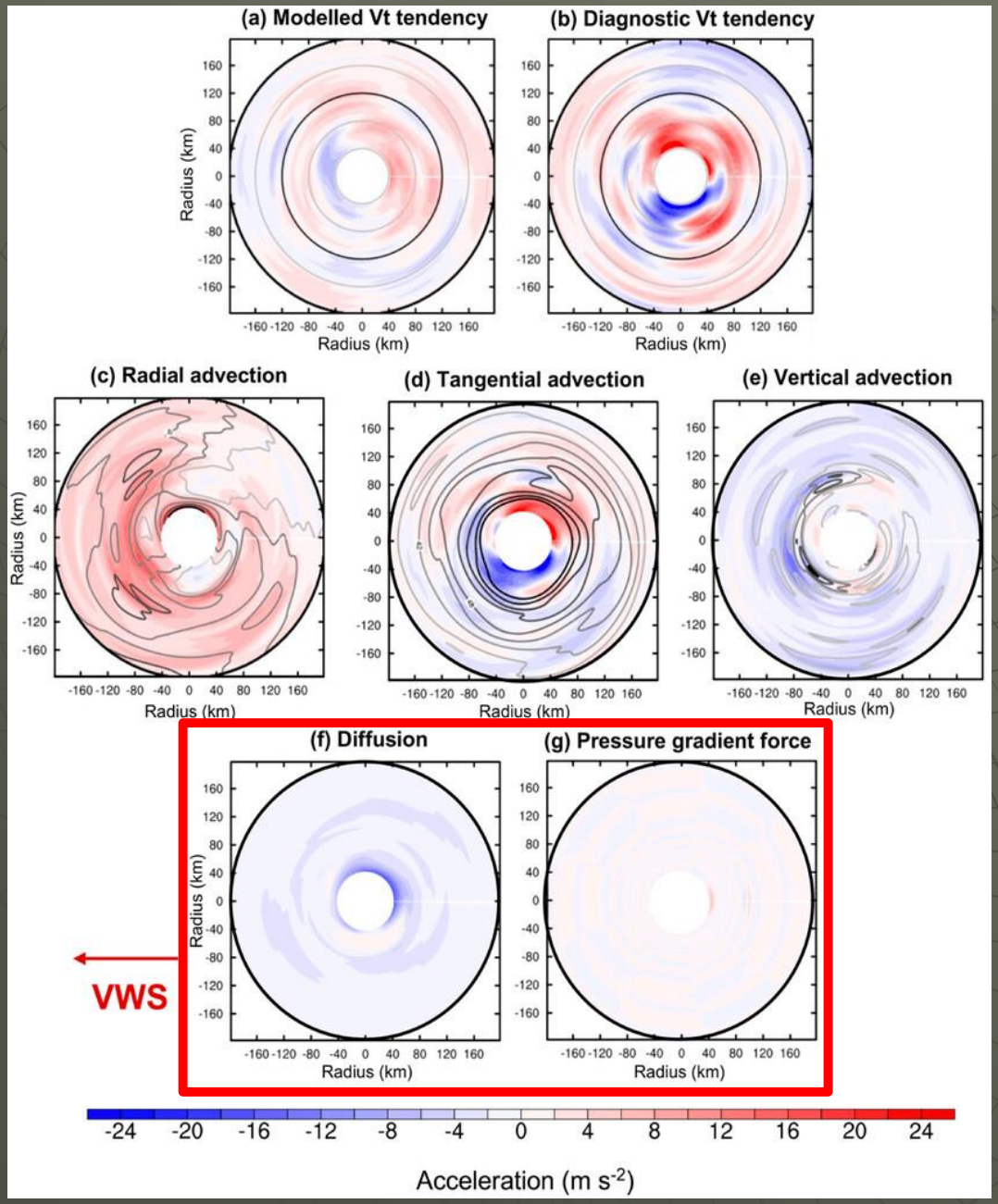

- Plan view of tangential wind budget at z = 1 km during 69–72 h in SH08: (a) modeled tangential wind tendency (m s^–1 h^–1), (b) calculated tangential wind speed tendency (m s^–1 h^–1), (c) radial advection term (m s^–1 h^–1, shading) and mean radial velocities (contours from 2 to 8 at 2 m s^–1 interval) during 69–72 h, (d) tendency of tangential advection (m s^–1 h^–1, shading) and mean tangential wind speed (contours from 39 to 60 at 3 m s^–1 interval), (e) vertical advection term (m s^–1 h^–1, shading) and mean vertical velocities (contours from 0.25 to 1 at 0.25 m s^–1 interval), (f) diffusion term (m s^–1 h^–1), and (g) tangential pressure gradient force (m s^–1 h^–1). The red arrow in the bottom left denotes the shear direction. Values within 40 km radius are omitted.

6. Discussion and Conclusions

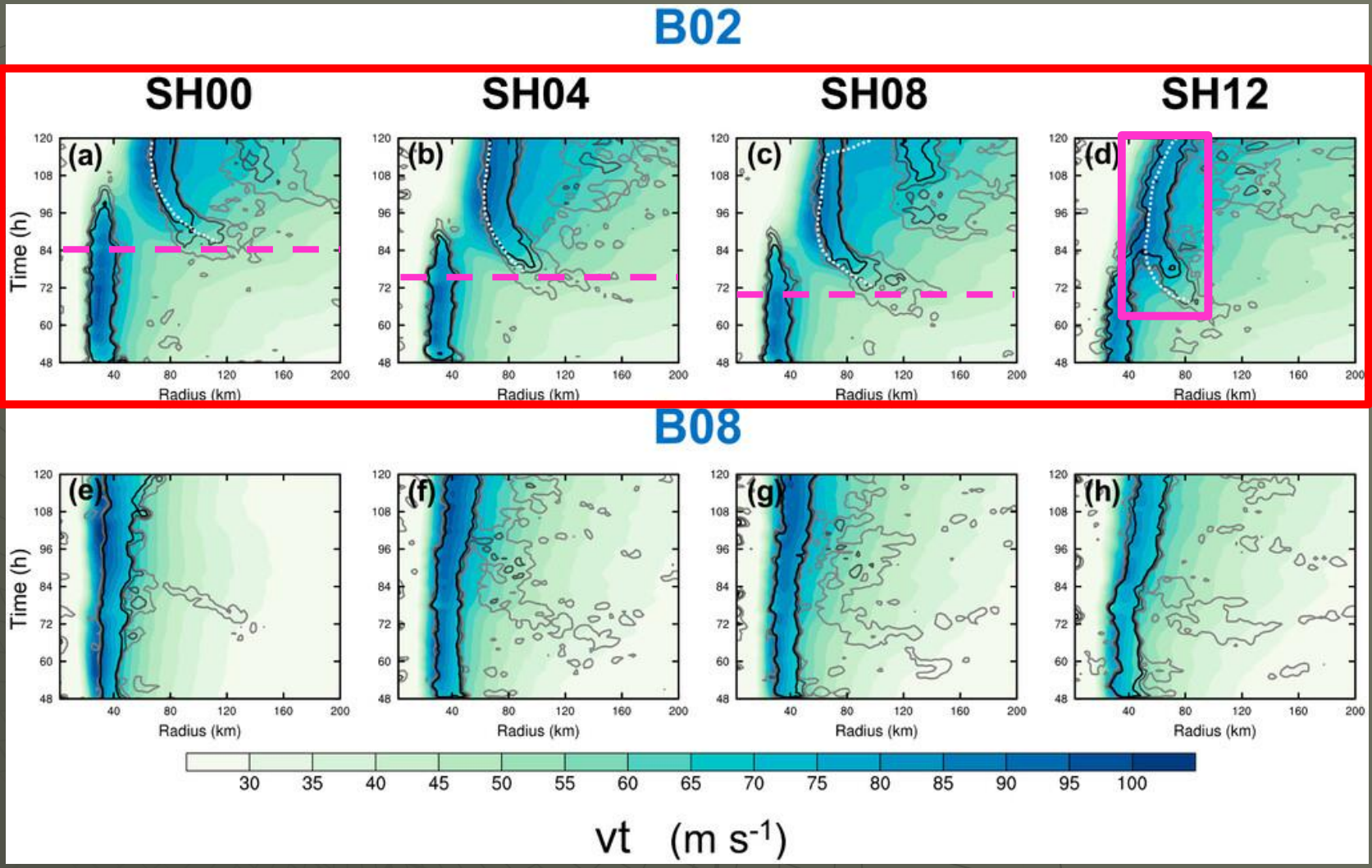

- (a)–(d) Time–radius evolution of the azimuthal-mean tangential wind at z = 1 km (m s^−1, shading) overlaid with the vertical velocity z = 5 km (m s^−1, contours at 0.25, 0.5, and 1.0 m s^−1) during 48–120 h for B02 group. (e)–(h) As in (a)–(d), but for B08 group. The secondary RMW is marked by white dashed lines.

6. Discussion and Conclusions cont.

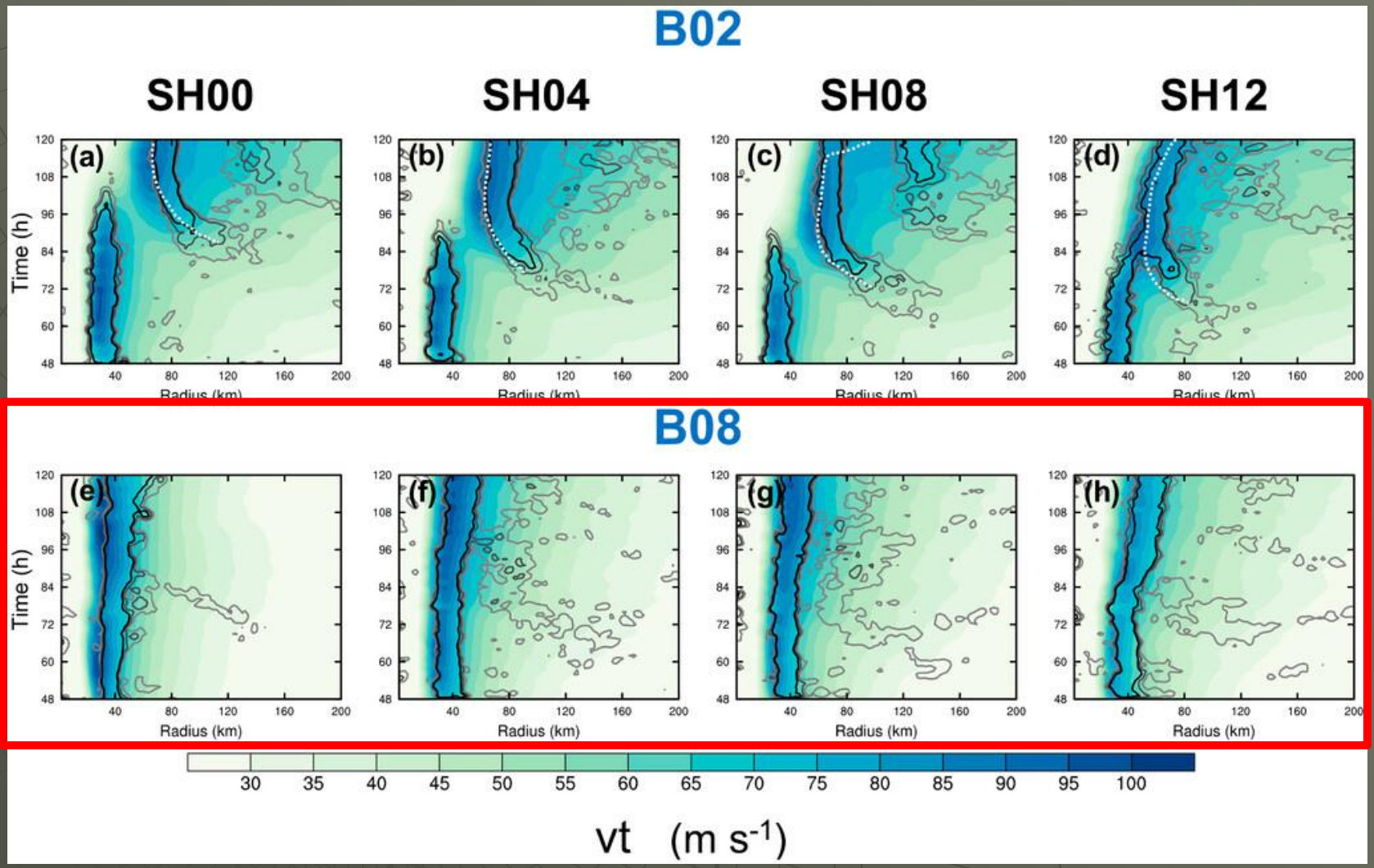

- (a)–(d) Time–radius evolution of the azimuthal-mean tangential wind at z = 1 km (m s^−1, shading) overlaid with the vertical velocity z = 5 km (m s^−1, contours at 0.25, 0.5, and 1.0 m s^−1) during 48–120 h for B02 group. (e)–(h) As in (a)–(d), but for B08 group. The secondary RMW is marked by white dashed lines.

6. Discussion and Conclusions cont.

- The results show that the effects of VWS on SEF is bifurcated depending on shear magnitudes. Weak-to-moderate VWS advances the timing of SEF while decreasing the radius of secondary tangential wind maximum. Strong VWS, however, causes significant TC weakening and breaks the secondary convective ring and therefore is unfavorable for SEF.

- At DR with the most favorable thermodynamic conditions, active convective cells form the upwind portion of ORBs. In the DL, convective cells gathered and matured, forming the middle portion of ORBs. Compared to the inner rainbands in the experiment without VWS, the stronger diabatic heating of ORBs in the DL quadrant under moderate VWS induces stronger BL inflow and radial convergence in SEF region.

- At UL where thermodynamic conditions for convection are reduced, the downwind end of ORBs exhibits obvious stratiform features. The asymmetric inflow induced by diabatic cooling descends from 6 km height into BL along the outer edge of the stratiform deck, reinforcing radial BL convergence at the radially inward side of ORBs. Radial BL convergence enhances convection of ORBs in return, resulting in increased BL inflow and accelerated low-level tangential wind jet. The positive feedback between ORBs and BL convergence promotes the enhancement of convection outside the primary eyewall and spinup of low-level tangential wind in the UL.

6. Discussion and Conclusions cont.

- It turns out the BL inflow in UL accelerates tangential wind through radial advection of absolute vorticity. The tangential wind jet transports increased tangential momentum downwind, accelerating the tangential wind and forming supergradient winds above the BL in the UR. As the downwind end of ORBs extends to UR, the pre-existing supergradient winds strengthen the low-level convection of ORBs, resulting in enhanced diabatic heating at UR. The initiation/enhancement of convection in UR promotes the closing of the secondary convective ring. Following that, enhanced BL inflow and acceleration of tangential wind are projected onto the azimuthal-mean state, forming the secondary tangential wind maximum.

- This study also looks into the negative effects of strong VWS on SEF. It turns out that convective downdrafts in DL bring low θe into the BL. The low-θe air is advected farther downwind, causing decreased instability and negative thermal buoyancy in UL. As a result, the stratiform precipitation in UL is weakened due to suppressed convective activities, thus cutting off the ORBs extending to upshear side.

- This study also reveals that in addition to the magnitudes of VWS, the effects of VWS on SEF also depend on vortex outer-core size. It is found that vortex with larger outer-core size has a higher resistance to VWS in terms of SEF.


The End…
Thanks !
Questions??